Calibration and Analysis of the GCT Camera for the Cherenkov Telescope Array

Jason J. Watson

Brasenose College
University of Oxford

A thesis submitted for the degree of
Doctor of Philosophy

Trinity 2018

Abstract

Lorem ipsum dolor sit amet, consectetur adipiscing elit. Pellentesque sit amet nibh volutpat, scelerisque nibh a, vehicula neque. Integer placerat nulla massa, et vestibulum velit dignissim id. Ut eget nisi elementum, consectetur nibh in, condimentum velit. Quisque sodales dui ut tempus mattis. Duis malesuada arcu at ligula egestas egestas. Phasellus interdum odio at sapien fringilla scelerisque. Mauris sagittis eleifend sapien, sit amet laoreet felis mollis quis. Pellentesque dui ante, finibus eget blandit sit amet, tincidunt eu neque. Vivamus rutrum dapibus ligula, ut imperdiet lectus tincidunt ac. Pellentesque ac lorem sed diam egestas lobortis.

Suspendisse leo purus, efficitur mattis urna a, maximus molestie nisl. Aenean porta semper tortor a vestibulum. Suspendisse viverra facilisis lorem, non pretium erat lacinia a. Vestibulum tempus, quam vitae placerat porta, magna risus euismod purus, in viverra lorem dui at metus. Sed ac sollicitudin nunc. In maximus ipsum nunc, placerat maximus tortor gravida varius. Suspendisse pretium, lorem at porttitor rhoncus, nulla urna condimentum tortor, sed suscipit nisi metus ac risus.

Aenean sit amet enim quis lorem tristique commodo vitae ut lorem. Duis vel tincidunt lacus. Sed massa velit, lacinia sed posuere vitae, malesuada vel ante. Praesent a rhoncus leo. Etiam sed rutrum enim. Pellentesque lobortis elementum augue, at suscipit justo malesuada at. Lorem ipsum dolor sit amet, consectetur adipiscing elit. Praesent rhoncus convallis ex. Etiam commodo nunc ex, non consequat diam consectetur ut. Pellentesque vitae est nec enim interdum dapibus. Donec dapibus purus ipsum, eget tincidunt ex gravida eget. Donec luctus nisi eu fringilla mollis. Donec eget lobortis diam.

Suspendisse finibus placerat dolor. Etiam ornare elementum ex ut vehicula. Donec accumsan mattis erat. Quisque cursus fringilla diam, eget placerat neque bibendum eu. Ut faucibus dui vitae dolor porta, at elementum ipsum semper. Sed ultrices dui non arcu pellentesque placerat. Etiam posuere malesuada turpis, nec malesuada tellus malesuada.

Calibration and Analysis of the GCT Camera for the Cherenkov Telescope Array

Jason J. Watson

Brasenose College

University of Oxford

A thesis submitted for the degree of

Doctor of Philosophy

Trinity 2018

Acknowledgements

Personal

Lorem ipsum dolor sit amet, consectetur adipiscing elit. Vestibulum feugiat et est at accumsan. Praesent sed elit mattis, congue mi sed, porta ipsum. In non ullamcorper lacus. Quisque volutpat tempus ligula ac ultricies. Nam sed erat feugiat, elementum dolor sed, elementum neque. Aliquam eu iaculis est, a sollicitudin augue. Cras id lorem vel purus posuere tempor. Proin tincidunt, sapien non dictum aliquam, ex odio ornare mauris, ultrices viverra nisi magna in lacus. Fusce aliquet molestie massa, ut fringilla purus rutrum consectetur. Nam non nunc tincidunt, rutrum dui sit amet, ornare nunc. Donec cursus tortor vel odio molestie dignissim. Vivamus id mi erat. Duis porttitor diam tempor rutrum porttitor. Lorem ipsum dolor sit amet, consectetur adipiscing elit. Sed condimentum venenatis consectetur. Lorem ipsum dolor sit amet, consectetur adipiscing elit.

Aenean sit amet lectus nec tellus viverra ultrices vitae commodo nunc. Mauris at maximus arcu. Aliquam varius congue orci et ultrices. In non ipsum vel est scelerisque efficitur in at augue. Nullam rhoncus orci velit. Duis ultricies accumsan feugiat. Etiam consectetur ornare velit et eleifend.

Suspendisse sed enim lacinia, pharetra neque ac, ultricies urna. Phasellus sit amet cursus purus. Quisque non odio libero. Etiam iaculis odio a ex volutpat, eget pulvinar augue mollis. Mauris nibh lorem, mollis quis semper quis, consequat nec metus. Etiam dolor mi, cursus a ipsum aliquam, eleifend venenatis ipsum. Maecenas tempus, nibh eget scelerisque feugiat, leo nibh lobortis diam, id laoreet purus dolor eu mauris. Pellentesque habitant morbi tristique senectus et netus et malesuada fames ac turpis egestas. Nulla eget tortor eu arcu sagittis euismod fermentum id neque. In sit amet justo ligula. Donec rutrum ex a aliquet egestas.

Institutional

Lorem ipsum dolor sit amet, consectetur adipiscing elit. Ut luctus tempor ex at pretium. Sed varius, mauris at dapibus lobortis, elit purus tempor neque, facilisis sollicitudin felis nunc a urna. Morbi mattis ante non augue blandit pulvinar. Quisque nec euismod mauris. Nulla et tellus eu nibh auctor malesuada quis imperdiet quam. Sed eget tincidunt velit. Cras molestie sem ipsum, at faucibus quam mattis vel. Quisque vel placerat orci, id tempor urna. Vivamus mollis, neque in aliquam consequat, dui sem volutpat lorem, sit amet tempor ipsum felis eget ante. Integer lacinia nulla vitae felis vulputate, at tincidunt ligula maximus. Aenean

venenatis dolor ante, euismod ultrices nibh mollis ac. Ut malesuada aliquam urna, ac interdum magna malesuada posuere.

Abstract

Lorem ipsum dolor sit amet, consectetur adipiscing elit. Pellentesque sit amet nibh volutpat, scelerisque nibh a, vehicula neque. Integer placerat nulla massa, et vestibulum velit dignissim id. Ut eget nisi elementum, consectetur nibh in, condimentum velit. Quisque sodales dui ut tempus mattis. Duis malesuada arcu at ligula egestas egestas. Phasellus interdum odio at sapien fringilla scelerisque. Mauris sagittis eleifend sapien, sit amet laoreet felis mollis quis. Pellentesque dui ante, finibus eget blandit sit amet, tincidunt eu neque. Vivamus rutrum dapibus ligula, ut imperdiet lectus tincidunt ac. Pellentesque ac lorem sed diam egestas lobortis.

Suspendisse leo purus, efficitur mattis urna a, maximus molestie nisl. Aenean porta semper tortor a vestibulum. Suspendisse viverra facilisis lorem, non pretium erat lacinia a. Vestibulum tempus, quam vitae placerat porta, magna risus euismod purus, in viverra lorem dui at metus. Sed ac sollicitudin nunc. In maximus ipsum nunc, placerat maximus tortor gravida varius. Suspendisse pretium, lorem at porttitor rhoncus, nulla urna condimentum tortor, sed suscipit nisi metus ac risus.

Aenean sit amet enim quis lorem tristique commodo vitae ut lorem. Duis vel tincidunt lacus. Sed massa velit, lacinia sed posuere vitae, malesuada vel ante. Praesent a rhoncus leo. Etiam sed rutrum enim. Pellentesque lobortis elementum augue, at suscipit justo malesuada at. Lorem ipsum dolor sit amet, consectetur adipiscing elit. Praesent rhoncus convallis ex. Etiam commodo nunc ex, non consequat diam consectetur ut. Pellentesque vitae est nec enim interdum dapibus. Donec dapibus purus ipsum, eget tincidunt ex gravida eget. Donec luctus nisi eu fringilla mollis. Donec eget lobortis diam.

Suspendisse finibus placerat dolor. Etiam ornare elementum ex ut vehicula. Donec accumsan mattis erat. Quisque cursus fringilla diam, eget placerat neque bibendum eu. Ut faucibus dui vitae dolor porta, at elementum ipsum semper. Sed ultrices dui non arcu pellentesque placerat. Etiam posuere malesuada turpis, nec malesuada tellus malesuada.

Contents

List of Figures

Abbreviations

AC Alternating Current.

ADC Analogue-to-Digital Converter.

ASIC Application-Specific Integrated Circuit.

CHEC Compact High Energy Camera.

CHEC-M Compact High Energy Camera (CHEC) using Multi-Anode Photomultiplier Tubes (MAPMTs) as the detector.

CHEC-S CHEC using Silicon Photomultiplier Tubes (SiPMTs) as the detector.

CTA Cherenkov Telescope Array.

DC Direct Current.

DCR Dark-Count Rate.

FEE Front-End Electronics.

FITS Flexible Image Transport System.

FPGA Field-Programmable Gate Array.

GCT Gamma-ray Cherenkov Telescope.

H.E.S.S. High Energy Stereoscopic System.

IACT Imaging Atmospheric Cherenkov Telescope.

MAPMT Multi-Anode Photomultiplier Tube.

MST Medium Size Telescope.

NSB Night-Sky Background.

PDE Photon Detection Efficiency.

PMT Photomultiplier Tube.

SCT Schwarzschild-Couder Telescope.

SiPMT Silicon Photomultiplier Tube.

SPE Single Photo-Electron.

SWIG Simplified Wrapper and Interface Generator.

TARGET TeV Array Readout with GSa/s sampling and Event Trigger.

TARGET 5 TARGET (TeV Array Readout with GSa/s sampling and Event Trigger) (version 5).

TARGET C TARGET (version C).

TIO Custom fits file format defined by TargetIO used for storing waveform data from TARGET-based cameras.

Vped Pedestal voltage input into the TARGET ASIC.

1

Introduction

Contents

:

1.1 Plan

1.1.1 Topics

- High Energy Astrophysics
  - Fermi
  - Fermi Bubbles
  - HAWC
- IACTs
- CTA
- CTA Science
  - Science Cases
  - Use "Science with CTA" paper
- SSTs
- SST Science
  - What do we contribute?
  - What can't be done without us?
- GCT
- CHEC
  - What makes us better?
  - Advantages of Schwarzchild-Couder
    - Increased FoV
    - Size
    - Cost
  - Advantages of full waveform readout
  - Other Advantages?
    - Trigger
    - Energy/power/voltage Requirements
    - Commonalities (SCT)

1.1.2 Questions

- ?

Shower properties, photons from bottom of shower are received before those at the top as the particle travels faster than light. Good figure in [1]

Gamma/Hadron/Lepton

Terminology note: charge not used in terms of columns, it refers to counts of photoelectrons, for which mV and ADC are a proxy of. Do a ctrl-f at end to check how charge is used

2

Camera Design & Mechanics

Contents

:

2.1 Plan

2.1.1 Topics

- Introduce TARGET architecture & Wilkinson ADC
- Different TARGET versions
- FEE
- MAPMs
- SiPMS
  - How they work
  - Comparison investigations
  - Property trade-offs
- CHEC-M
- Changes for CHEC-S
- Future - MUSIC ASICs

2.1.2 Questions

- ?

2.2 Introduction

:

- number of pixels
- number of modules
- number of pixels per module
- number of cells
- pixel gaps
- module gaps

2.3 CHEC-M

schematic illustration of electronics

2.3.1 Multi-Anode Photomultiplier Tubes

connection between gain and hv

table of parameters

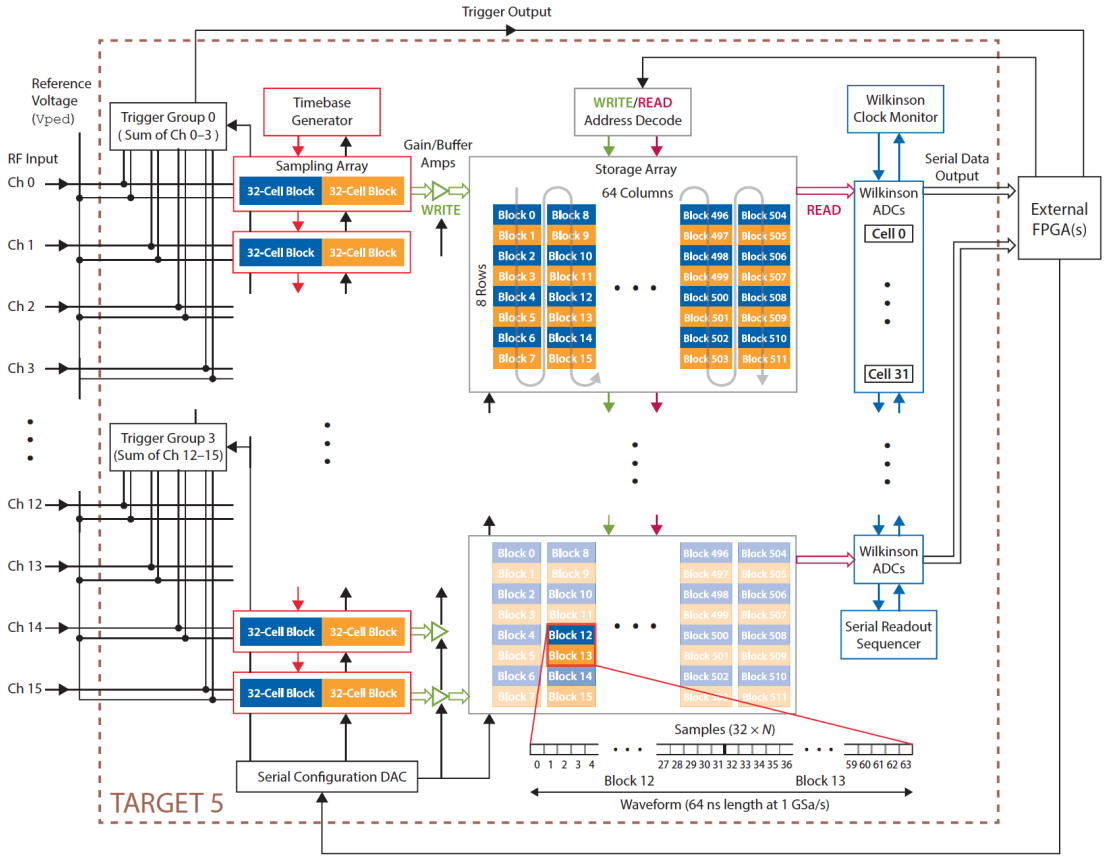

Figure 2.1: Functional block diagram of the TARGET 5 ASIC [2]

Add more details

2.3.2 Front-End Electronics

Pre-Amplifiers

TARGET

2.3.3 Back-End Electronics

Backplane

DACQ Boards

2.4 CHEC-S

2.4.1 Silicon Photomultipliers

connection between gain and bias voltage

table of parameters

2.4.2 TARGET-C

larger dynamic range, reference tf plot????

name of TARGET-C FPGA?

2.5 External Components

2.5.1 LED Flashers

2.5.2 Chiller

2.6 Future

2.7 Laboratory Set-Up

2.8 Laboratory Calibration

In order to obtain reliable knowledge on the average illumination incident on the camera in our laboratory, we must calibrate the laser and filter wheel combination. This is of paramount importance for performing the camera flat-field calibration, and for obtaining a laboratory charge resolution result. There are four stages required to achieve a calibration from filter-wheel position to expected charge in each pixel:

1. Measuring the relationship between filter-wheel position and light transmissivity.

2. Measuring the relative amount of light each pixel receives due to its position on the focal surface.

3. Measuring an absolute illumination in photoelectrons for at-least one filter-wheel position.

From the combination of these results, we are able to obtain a conversion from filter-wheel position to expected number of photoelectrons in each pixel.

2.8.1 Filter Wheel

Using a single reference silicon photomultiplier pixel connected to an oscilloscope, centred on the camera focal plane, the ratio between the pulse area with and without the neutral-density filter was calculated for different filter-wheel positions (i.e. different filter levels). The filter-wheel positions 100 to 3025 are utilised to cover the full dynamic range of the camera, within which the transmission is expected

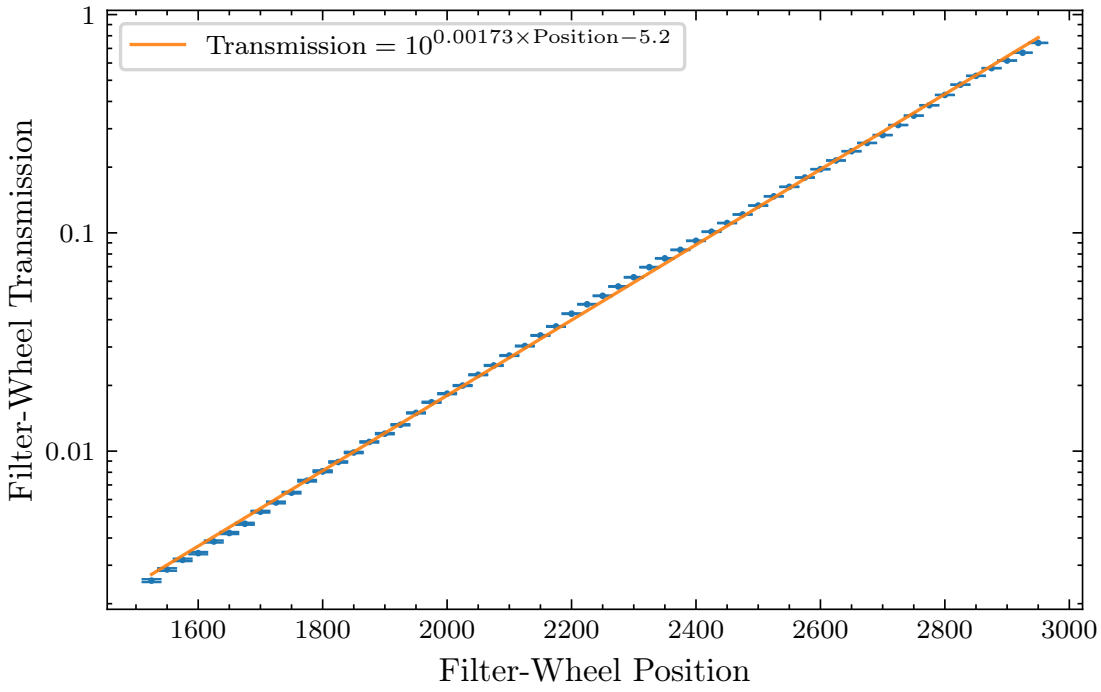

Figure 2.2: Logarithm of transmission versus position for the filter wheel. The relationship is fit with a straight line.

Figure 2.3: Spatial profile of the laser illumination along a flat plane in front of the camera, measured with a single reference SiPMT pixel attached to a robot arm.
Show value in each position, and then gradient fit?

.

to increase logarithmically with position. With the transmission axis in log-space, the relationship between filter-wheel position and transmission is obtained using a linear regression of the data points (Figure 2.2), which can be extrapolated to the lower values of filter-wheel position. Only the positions 1525 to 2950 are shown in this calibration, due to the signal at lower positions being too small to reliably measure with the combination of approach and reference SiPMT. Future repeats of this calibration will use a different sensor or additional methods in order to explore the full range of filter-wheel position.

2.8.2 Illumination Profile

There exists two contributions to the relative amount of light each pixel receives, depending on the position of the pixel.

Laser Profile

Despite attempts to homogenise the illumination from the laser plus diffuser, there are still non-uniformities in the light received at the camera pixels that should be corrected for in the calibration. As shown in Figure 2.3, a linear gradient in laser illumination exists across the x-y plane. This was found by attaching a single silicon photomultiplier pixel to a robot arm at the same distance from the laser as the camera. By using a single pixel the amplitude measured is disentangled from the relative PDE. This pixel was then moved to an x-y position to calculate the ratio in signal amplitude, returning back to the origin to obtain a fresh value to compare to, thereby correcting for any deviations due to a change in temperature. The resulting distribution of ratios was fit with a linear gradient across the plane.

Camera Geometry

Due to the spherical camera focal surface, each pixel is at a different distance d_z from the light-source, and therefore receives a different amount of light depending on its distance x from the camera centre. Furthermore, the "viewing area" A_V of the pixel from the light-source reduces with distance from the camera centre as the tangent to the pixels approximately align with the tangent to the curved camera focal surface, creating the "viewing angle" β between the tangent and direction to the light-source. The combined geometric correction to the light intensity required to compensate for these effects is circularly symmetric, and therefore can be analytically approximated by using a two dimensional description of the camera, with a circular focal surface:

$$d_1 = r - d_2 = r - \sqrt{r^2 + x^2}, \tag{2.8.2.1}$$

$$d_z = \sqrt{x^2 + (d_c + d_1)^2} = \sqrt{x^2 + (d_c + r - \sqrt{r^2 + x^2})^2}. \tag{2.8.2.2}$$

$$\beta = \theta + \alpha = \sin^{-1}\frac{x}{d_z} + \sin^{-1}\frac{x}{r}, \tag{2.8.2.3}$$

$$\frac{A_V}{A_P} = \cos\beta, \tag{2.8.2.4}$$

$$\frac{I_x}{I_c} = \frac{d_z^2}{d_c^2} \times \cos\beta, \tag{2.8.2.5}$$

where A_P is the pixel area, I_x is the intensity measured at the position of the pixel, I_c is the intensity measured at the centre of the camera, and the remaining distances and angles are shown in Figure 2.4.

The resulting geometry corrections to the intensity for each pixel, arising from Equation2.8.2.5, can be seen in Figure . add figure

The final illumination profile correction, combining both the laser profile and camera geometry, can be seen in Figure . add figure

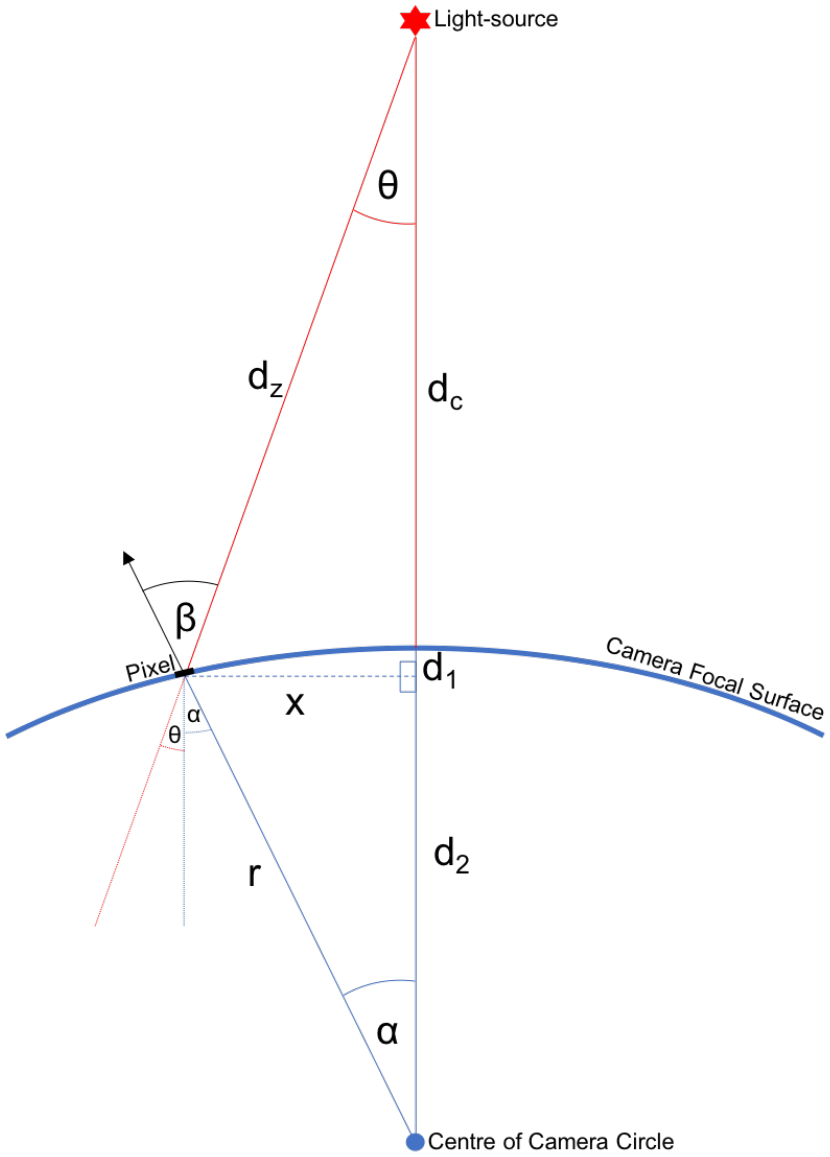

Figure 2.4: Two-dimensional geometry schematic of the laboratory set-up for uniform camera illumination, used to calculate the reduction in light level for each pixel depending on its distance from the camera centre.

2.9 Absolute Illumination

The method adopted to obtain a value for the absolute illumination is to use a fit to the Single Photoelectron spectrum resulting from low-amplitude illumination of the pixels. Contained within this fit is the average illumination parameter, λ. This topic is further covered in Chapter 5.

By simultaneously fitting 3 illuminations, we obtain 3 values of λ per pixel. With the 3 filter-wheel transmissions (corresponding to the 3 illuminations) on the x-axis, these values of λ can be linearly regressed to obtain the gradient M_λ and

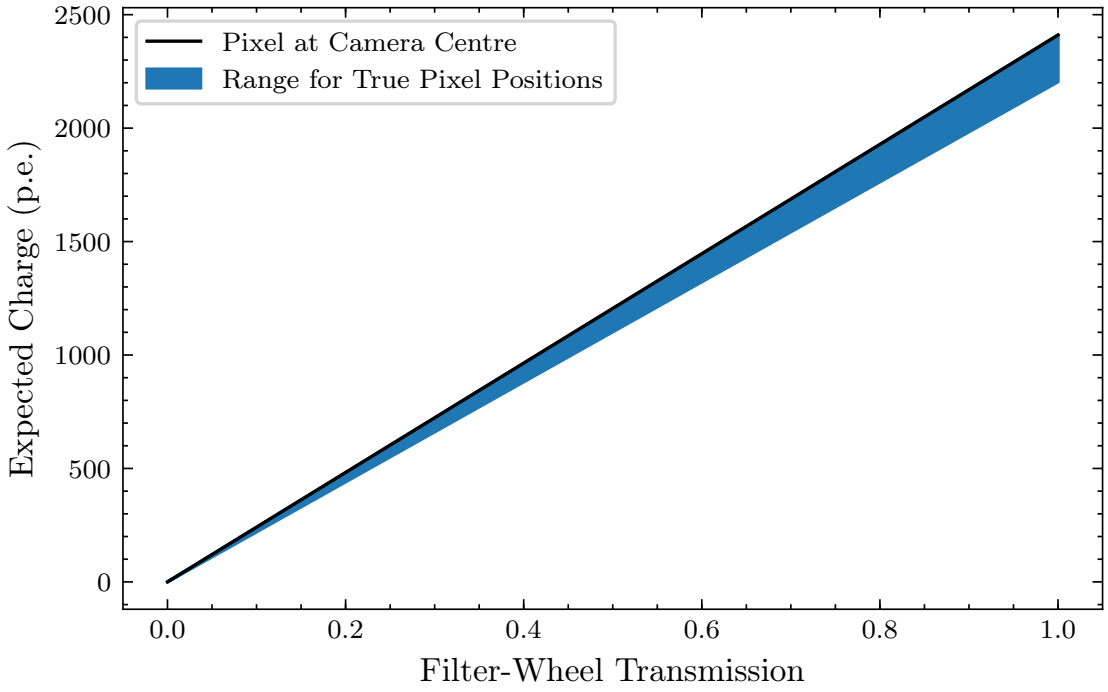

Figure 2.5: Relationship between filter-wheel transmission and expected charge in photoelectrons resulting from the filter-wheel calibration. The black line shows the conversion for a theoretical pixel exactly positioned at the camera centre. The blue segment shows the range for the actual pixels in the camera, with the consideration of illumination profile included.

y-intercept C_λ per pixel. The y-intercept represents the λ you would get with zero filter-wheel transmission, and therefore indicates the Night-Sky Background (NSB) and Dark-Count Rate (DCR). The variation in M_λ across the pixels arises from the folding of the illumination profile and the relative Photon Detection Efficiency (PDE). Therefore, the next step is to correct for the illumination profile contribution to the gradient, the result of which is solely the relative PDE (Figure add figure, in this chapter or results chapter?). The calibration from filter-wheel transmission T_{FW} to average camera illumination $\bar{I}_{pe}$ is then:

$$\bar{I}_{pe} = \bar{M}_\lambda T_{\mathrm{FW}} + \bar{C}_\lambda, \tag{2.9.0.1}$$

2.9.1 Expected Charge

As we correct for the NSB in the extracted signal value (Section 5.4), the NSB contribution to Equation 2.9.1.1 ($\bar{C}_\lambda$) is subtracted to give us the charge we expect when illuminating the camera with a filter-wheel transmission T_{FW}, for a theoretical pixel perfectly positioned at the camera centre. To obtain the expected charge for

each true camera pixel $Q_{\mathrm{Exp}_{\mathrm{pix}}}$, this relation must be folded with the illumination profile correction factor F_{pix} to give:

$$Q_{\mathrm{Exp}_{\mathrm{pix}}} = \bar{M}_{\lambda} T_{\mathrm{FW}} F_{\mathrm{pix}}. \tag{2.9.1.1}$$

Figure 2.5 shows the relation between filter-wheel transmission and the expected charge for the camera pixels.

2.10 Readout Characteristics

define ADC

monitoring information

3

CTA Architecture

Contents

:

3.1 Plan

3.1.1 Topics

- Requirements
- Data Levels

3.1.2 Questions

- ?

3.2 Introduction

Due to the large scope of Cherenkov Telescope Array (CTA), in both its construction and operation, a formal approach towards a system architecture was adopted [3]. One important aspect within this architecture is the distinction between the CTA Consortium and the CTA Observatory. The CTA Consortium is a group of institutes responsible for directing the science goals of the observatory, and for developing software and hardware (including cameras), which are supplied to the observatory as

in-kind contributions. The consortium consists of 200 institutes across 31 countries [4]. Conversely, the CTA Observatory pertains to the major astronomical facility that serves science data to a wide user community as an open observatory. The CTA Observatory gGmbH is the legal entity for CTA in the preparation for the implementation of the CTA Observatory, and works in close cooperation with the consortium during this process [5].

The purpose of the *CTA Architecture* is to maintain communication and understanding among all CTA contributors during the pre-construction phase in order to ensure a coherent development process and seamless integration of the developed units into a whole. During this chapter I will describe two aspects of the *CTA Architecture* that are important in the context of this thesis: certain requirements that all cameras, including CHEC, must meet; and the descriptions of how camera-observation data are handled in CTA, including the system flow and data level definitions.

3.3 Requirements

In order to ensure the science goals of CTA are achievable, and that the observatory remains operational for the full 30 life-time, certain standards must be upheld by all components of the observatory; this is the purpose of the CTA requirements. The requirements cover every aspect of the observatory, including: the survival of environmental conditions (*B-ENV-0320 Survival humidity*), the time allowed by the analysis pipeline for processing (*A-OBS-0810 Data Processing Efficiency*), the reliability of telescope components (*B-TEL-0520 Structure Lifetime*), and the ability to meet the expected performance (*PROG-0025 Differential Sensitivity under Low Moonlight - North*). In order for an in-kind contribution to be accepted, it must meet the requirements defined by the observatory. These requirements are therefore the standards for which we compare the performance of CHEC against, and are the primary drivers in my development of the low-level calibration and analysis. However, there exists more than 60 requirements specifically tailored for the cameras. Consequently, the full review of the camera is a large undertaking that extends beyond the scope of this thesis. Instead, only the requirements that have relevance to the topic of this thesis are discussed.

It is important to note that the requirements, located on the CTA Jama website [6], are currently under-review and therefore subject to change. One such change that is under-way at the time of this writing is the redefinition from units of photoelectrons to photons. Originally, a common consolidated Photomultiplier

Tube (PMT) was envisioned to be used for all cameras in CTA, motivating for the expression of requirements to be in photoelectrons. However, due to the advances in sensor technology and the adoption of SiPMTs, this assumption has lead to problems with such a definition [7]. Firstly, a fixed NSB level defined in terms of photoelectrons does not allow for trade-offs between NSB acceptance and other performance parameters. Secondly, with an SiPMT-based camera it is possible to obtain a better Cherenkov intensity resolution and a lower energy threshold, but still fail the current requirements, whilst a camera design with inferior performance may pass. The current requirements could be met by a camera with subpar SiPMTs by reducing its bias voltage, which in turn reduces the optical cross-talk and photon detection efficiency, hence bringing the excess noise factor and threshold in photoelectron units down. While such a camera meets the current requirements, it is at the cost of performance in terms of photon intensity (and therefore Cherenkov-shower energy threshold).

talk with Tom about this, and how trigger efficiency was affected by being defined in p.e.

A copy of each requirement at the time of this writing is included alongside the discussion in this section to ensure clarity about which version of the requirement definition is being referred to. Future investigations should check the latest requirement definition.

3.3.1 B-TEL-1010 Charge Resolution

The required fractional Charge Resolution for Cherenkov signals in each Camera pixel for a specified background level of 0.125 photoelectrons/ns is given in the Figure below and Table attached. Charge measurements must be possible for 0-1000 photoelectron signals. The average charge resolution should be calculated for the reference Gamma-Ray Spectrum.

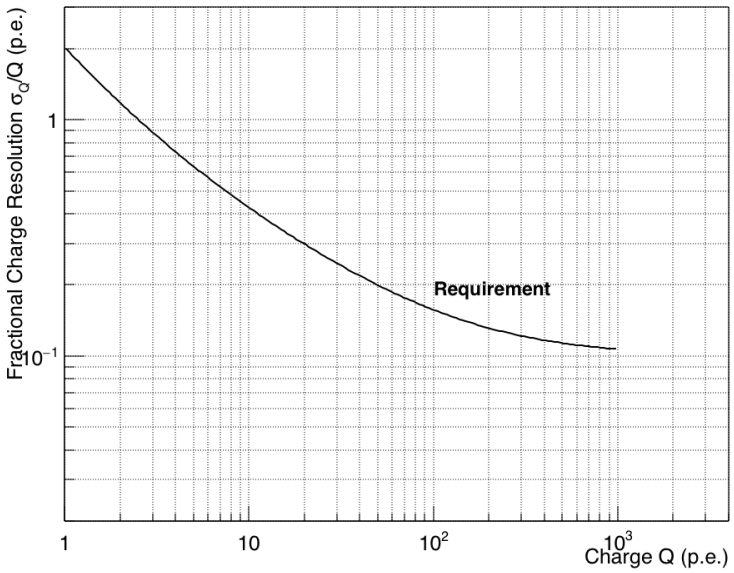

Figure 3.1: Fractional rms charge resolution σ_Q/Q per pixel for different Cherenkov light signal amplitudes, expressed in units of photoelectrons (p.e.). All sources of fluctuations, including Poisson fluctuations in photoelectron number, must be included, The true pixel charge Q is that measured in an ideal detector with the same photon-detection efficiency.

Notes: It is expected that this requirement is verified with reference to:

- Monte Carlo simulation of Cherenkov light from gamma-ray initiated showers (using a verified telescope model),
- Level-C Specification on Laboratory Measured Charge Resolution,
- Monte Carlo simulation of the laboratory test set-up (as a means of telescope model verification).

Note that between 1000 p.e. and 2000 p.e., some sensitivity to increasing input signal must exist.
This requirement applies to post-calibration (DL1) data.
Note that this requirement will likely need to be expanded to cover performance at higher NSB levels.

519

Definition

The standard criterion for low-level performance used in CTA is the *Charge Resolution*. It encompasses both the bias and the standard deviation of the extracted charge versus the expected charge to provide a measure of the waveform, calibration, and charge reconstruction quality. Analogous to the Root-Mean-Square Error, the fractional *Charge Resolution* $\frac{\sigma_Q}{Q_T}$ for a particular "true charge" Q_T (the charge that would be measured directly after the photocathode of the sensor) is defined as

$$\frac{\sigma_Q}{Q_T} = \frac{1}{Q_T}\sqrt{\frac{\sum_{i=0}^{N}(Q_{M_i} - Q_T)^2}{N}}, \tag{3.3.1.1}$$

where N is the total number of measured charges, Q_{M_i}, with that value of Q_T. The associated CTA requirement defines the maximum allowed values of $\frac{\sigma_Q}{Q_T}$ for values of Q_T between 1-1000 p.e., which must be adhered to when resolving the signal for any camera in CTA.

Requirement Derivation

The uncertainty in charge reconstruction can be expressed in the form

$$\frac{\sigma_Q}{Q} = \frac{1}{Q}\sqrt{\sigma_0^2 + \sigma_{ENF}^2 Q + \sigma_g^2 Q^2}, \tag{3.3.1.2}$$

where σ_0 encapsulates noise contributions (electronic and NSB), $\sigma_{ENF} = 1 + ENF$ is determined from the *Excess Noise Factor* (a measure of the avalanche gain fluctuations), and σ_g is the multiplicative errors of the gain [7][8]. σ_0 can be further expanded in terms of the two primary noise contributions:

$$\sigma_0 = \sqrt{NSB \times t_w + n_e^2}, \tag{3.3.1.3}$$

i.e. the *NSB* rate (which includes the DCR for the purpose of this discussion) is coupled with the effective signal readout window size, $t_w = 15$ ns, and summed with the electronic noise, n_e. A contribution from electronic noise of $n_e = 0.87$ photoelectrons is assumed, combined with a value of $NSB = 0.125$ p.e./ns as defined in the requirement. A value of $\sigma_g = 0.1$ and $ENF = 0.2$ is also assumed [7]. The resulting combination of miscalibration and noise factors in Equation 3.3.1.2 gives the *Charge Resolution* requirement illustrated in Figure 3.1.

Approach

As it is impossible to know the "true charge" generated by a Cherenkov signal in the field, Monte Carlo simulations must be relied upon in order to prove a camera meets this requirement. The process for achieving this is outlined in the notes to the requirement. It is expected that this requirement is validated in three ways:

1. With lab measurements where the camera in uniformly illuminated with a calibrated light-source.

2. With simulations of the previous approach, in order to verify the simulation model of the camera.

3. With Monte Carlo simulations of Cherenkov signal incident on the full telescope model.

The final item is the most important in confirming the requirements are met, as temporally-uniform illuminations do not sufficiently test the ability to find the signal pulse in the waveforms for the case of a Cherenkov-shower illumination.

The software package *sim_telarray* (Chapter 4) stores the "true charge" generated after the photocathode for each shower event into the output file. Therefore, with an accurately simulation model of the camera, it is an appropriate package for investigating a camera's performance against this requirement. However, in order to ensure Poisson fluctuations in photoelectron number are included, as per the requirement, when using the "true charge" stored in the simulation file, the corrected form of Equation 3.3.1.1 is

$$\frac{\sigma_Q}{Q_T} = \frac{1}{Q_T}\sqrt{\frac{\sum_{i=0}^{N}(Q_{M_i} - Q_T)^2}{N} + Q_T}. \tag{3.3.1.4}$$

With the form in Equation 3.3.1.4, a perfect detector that consistently reads-out a "measured charge" with equal value to the "true charge" would hit the Poisson limit, as it is not physically possible to know the the "true charge" generated by the photocathode without fluctuations. The Poisson limit is shown alongside the *Charge Resolution* requirement in Figure .

figure showing the two limit lines

3.3.2 B-TEL-1295 Pixel Availability

During observations, at least 95% of all camera pixels must be available and usable for data analysis. In addition, continuous regions of non-functioning pixels must not exceed 2% of all camera pixels. Pixels excluded due to NSB levels beyond those required are not included in this budget.

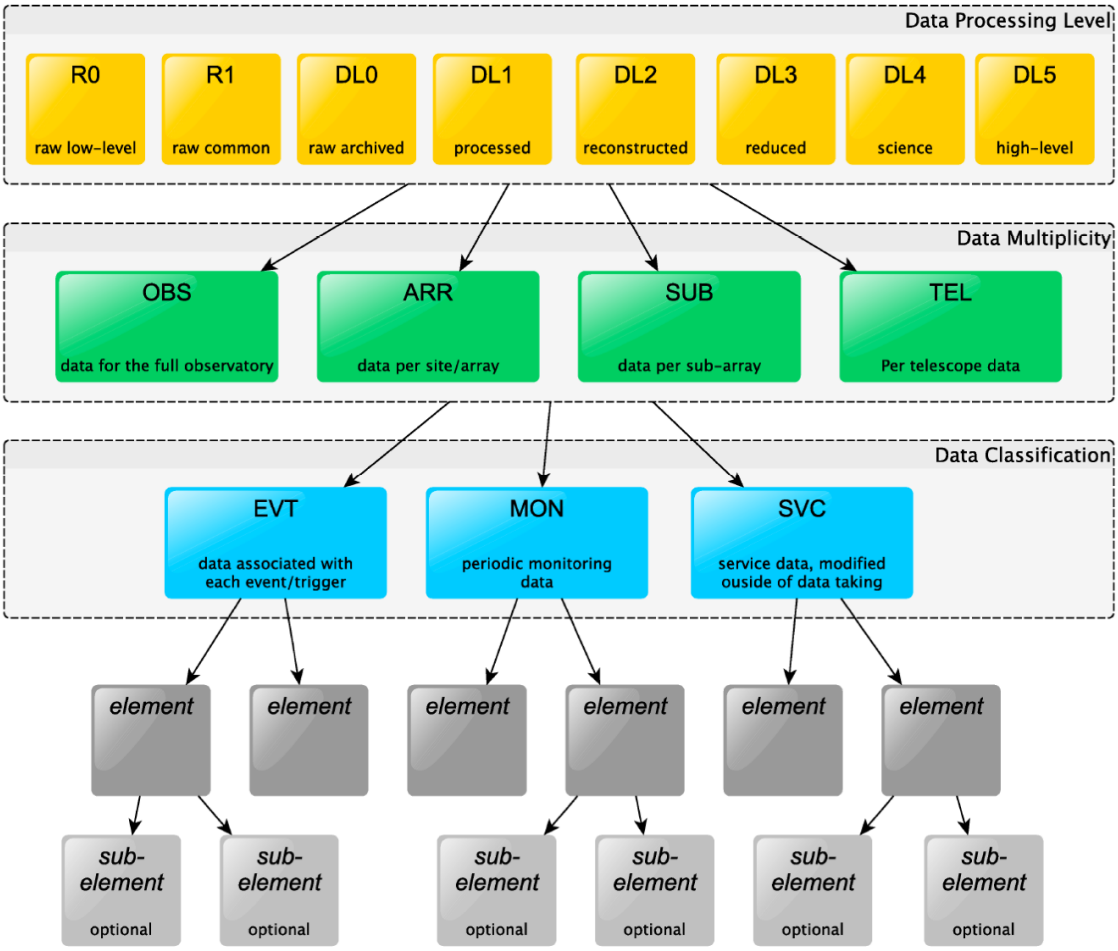

Figure 3.2: Hierarchy of data element names including the data level, the classifications of data (based on their rate), and data elements/groups and sub-elements/groups [9].

This requirement sets a limit on the amount of "dead" pixels that can be allowed on a camera before the entire camera is considered to be unavailable. For CHEC, which contains 2048 pixels, this imposes the following possible limitations:

- The camera may only have a maximum of 102 dead pixels. This allows 3 dead pixels per module.
- The amount of continuous pixels that are allowed to be dead is 41, therefore if a module dies, the camera's capabilities become insufficient for the CTA requirements. However, a maximum of two ASIC (Application-Specific Integrated Circuit)s are allowed to die.

3.4 Data Level and Flow Model

Another aspect of the *CTA Architecture* that is relevant to this work are the *Data Processing Level* definitions, and the flow between them. These definitions dictate

how the data obtained from the telescopes are handled within the observatory, and are important in ensuring each telescope adopts a similar processing chain to guarantee compatibility between themselves and the pipeline framework software.

Figure 3.2 shows the full hierarchy for data specification in the observatory. The *Data Processing Level* indicates the progression of the data along the processing chain, the *multiplicity* indicates the scope of the data, and the *classification* designates the type of the data [9]. As the primary focus of this thesis is on the individual telescopes waveform data, the rest of this section will be focussed on describing the data levels relevant to the *EVT*- classification, and the processes used to transition between them. This subject is still undergoing development within CTA, but the foundations are generally accepted. A simple overview of this topic is shown in Figure **??**.

R0 *(raw low-level)*: Raw waveform data, internal to the Camera Functional Unit.

R1 *(raw common)*: Waveform data with *R1 Calibration* applied. This low-level calibration is unique to the camera, to remove the dependence on the behaviour of its specific electronics. The CHEC *R1 Calibration* is described in Chapter 5. A selection of gain-channel is also performed for cameras with 2 channels. This level contains data which are serialised to a wire format, i.e. a block of data sent over a network in a common way between the telescopes. This data level is processed by the *Online Analysis* pipeline in order to produce immediate science alerts. The *R1* level therefore has its own *CTA Requirements* to adhere to (including its own *Charge Resolution* requirement), ensuring that the minimum standard required for the *Online Analysis* and *Data Volume Reduction* is met. Further (potentially slower) calibration may be applied at a later stage (*DL0* to *DL1a*) such that the results of the offline pipeline are of optimum quality.

DL0 *(raw archived)*: Similar data to the *R1* level, except serialised into files and are intended to be archived for the long-term. In order to achieve this with the excessively large data volume produced by CTA, *Data Volume Reduction* must be performed to achieve 2 orders of magnitude reduction. The simplest

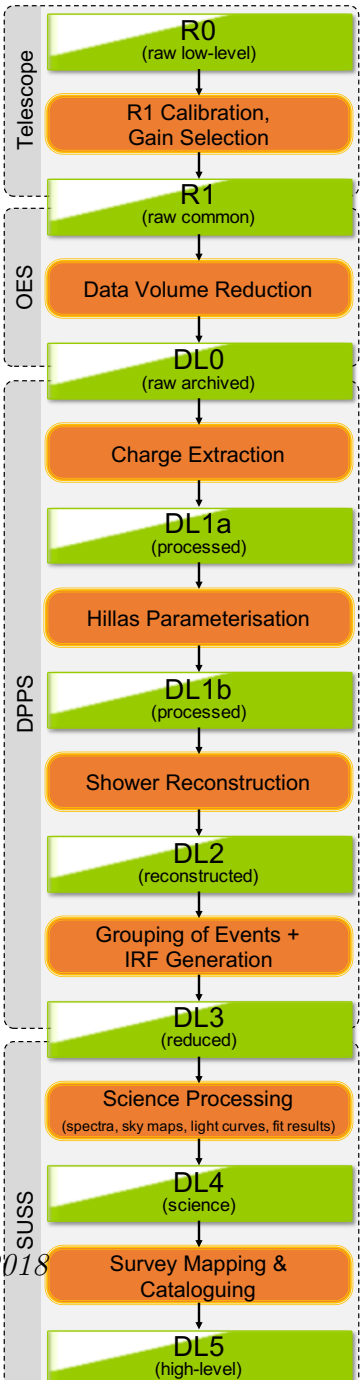

form of reduction is known as zero-suppression, where only waveforms of pixels deemed to have signal are kept, but more advanced forms of reduction are under investigation. This is one of the responsibilities of the Observation Execution System (OES).

find reference

DL1 *(processed)*: The signal charge is extracted from the *DL0* waveform data, and characterised in terms of its *Hillas Parameters*. This process is handled by the Data Processing and Preservation System (DPPS) offline data processing pipeline, of which `ctapipe` is a prototype of. Further information about `ctapipe` can be found in Chapter 4, and details about the processes in this stage are described in Chapter 6.

DL2 *(reconstructed)*: The *DL1* products (pixel charges and *Hillas Parameters*) are used to reconstruct shower parameters including energy, direction, and source particle. At this point, the *TEL multiplicity* is dropped, as the information from each telescope has been combined to perform the reconstruction, and the individual telescopes are no longer relevant. The operations involved in this stage are also performed by the DPPS offline pipeline, and are described in Chapter 6.

DL3 *(reduced)*: Events are sorted into sets according to their type (e.g. gamma-ray candidates, electron candidates, selected hadron candidates, etc.) alongside their reconstruction parameters. Associated instrumental response characterizations and any technical data needed for science analysis are also included in this level.

DL4 *(science)*: The *DL3* data are read into the one of the CTA tools within the Science User Support System (SUSS) designed to support science data analysis. Two prototype tools developed within this system are *gammapy* and *ctools* (Chapter 4). These tools provide enable the construction of binned data products like spectra, sky maps, or light curves. These can be fit against models to make conclusions about the astronomical source.

DL5 *(high-level)*: Accumulations of *DL4* data to generate CTA survey sky maps or the CTA source catalogue.

4

Software

Contents

:

4.1 Plan

4.1.1 Topics

- TargetIO/TargetDriver
- TargetCalib
- ctapipe
- gammapy/CTOOLS

4.1.2 Questions

- ?

4.2 Introduction

In Chapter 3, the data processing steps that are required in order to obtain the science data that is released by the CTA Observatory are described. In order to go from camera trigger to science results, a number of software packages must be developed, and be provided to CTA as in-kind contributions, as instructed by the CTA Architecture.

This chapter provides an outline of the software packages used in the pipeline for CHEC and CTA, alongside my contributions to them.

4.3 TARGET Libraries

A collection of libraries have been created to operate, readout, and calibrate the cameras containing TARGET modules (CHEC and the Schwarzschild-Couder Telescope (SCT) camera), and are therefore known as the "TARGET Libraries". These low-level libraries are wrote in C++as they prioritise efficiency over flexibility. To enable the use of these libraries from the Python packages used in waveform reduction, a Python wrapper for these libraries is automatically generated during compilation by SWIG (Simplified Wrapper and Interface Generator)[1].

These libraries are presently stored on the CTA-SVN version control server, and installation instructions can be found at `https://forge.in2p3.fr/projects/gct/wiki/Installing_CHEC_Software`, provided you have permissions to the Gamma-ray Cherenkov Telescope (GCT) Redmine.

4.3.1 `TargetDriver`

In order to operate, or "drive", the TARGET modules, the `TargetDriver` library is required. This C++library configures the TARGET modules, and listens for the UDP packets containing the waveform data.

4.3.2 `TargetIO`

The file format used to store waveforms from TARGET modules is a custom FITS (Flexible Image Transport System) format defined by `TargetIO`, hereby referred to as the TIO) format. This library is always used to read and write waveform and header (information such as observation time) data to the TIO file. TIO files can either contain *R0* (uncalibrated) or *R1* (low-level calibrated) waveform

[1] http://www.swig.org/

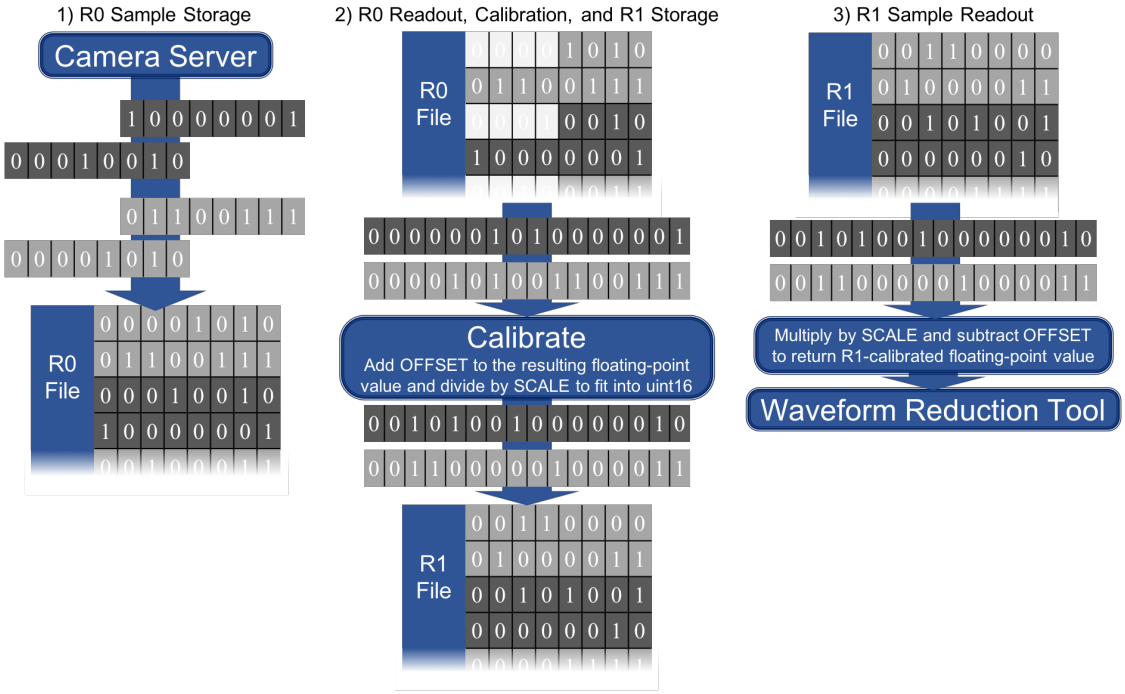

Figure 4.1: Simple overview of the data-flow for waveform samples within the TARGET libraries:

1) 8-bit/char packets are sent from the TARGET FPGA and stored directly to file. A waveform sample is 12-bit, therefore the first four bits of the first 8-bit sample packet are used to indicate sample order.

2) When reading a sample from the R0 TIO file, the first four bits are ignored, and the remaining twelve bits are combined into an unsigned 16-bit sample. The samples are passed to `TargetCalib` for calibration. The resulting calibrated floating-point sample is scaled and offset to fit into an unsigned 16-bit integer for storage.

3) When reading a sample from a R1 TIO file, the entirety of the two 8-bit packets are kept and combined. The value is returned to floating-point format using the OFFSET and SCALE stored in the file header.

Although only the samples are shown here, all other waveform data is also sent along this stream, including ASIC and Channel number, indicating the start of a new waveform.

data. Each sample in a waveform is stored to file as an unsigned 16-bit integer. The raw waveform digital counts measured by the camera are serialised in an unsigned 12-bit integer format, and the data packets received from the TARGET Field-Programmable Gate Array (FPGA) are 8-bit in size, therefore the first 4 bits of a waveform sample inside an *R0* TIO file are not used. When storing calibrated waveforms, the post-calibration floating-point sample is scaled and offset to fit the full 16-bit unsigned integer. These scale and offset values are stored in the file header and automatically applied to convert the sample back into floating-point format when read. Figure 4.1 demonstrates the data-flow processes involving the TIO files.

To ensure the full efficiency of the C++library is exploited via the Python wrapper, I contributed the `WaveformArrayReader` class, which, when passed a contiguous block of memory (such as a `numpy.array`), promptly fills the array with the entire camera's waveform data for that event. For example, to read an *R1* TIO file from Python:

```
1  import numpy as np
2  from target_io import WaveformArrayReader
3
4  # Create the reader and get the number of pixels and number of
       samples from the header
5  reader = WaveformArrayReader("/path/to/file/Run17473_r1.tio")
6  n_pixels = reader.fNPixels
7  n_samples = reader.fNSamples
8
9  # Generate the memory to be filled in-place
10 waveforms = np.zeros((n_pixels, n_samples), dtype=np.float32)
11 first_cell_ids = np.zeros(n_pixels, dtype=np.uint16)  # Storage
       cell id for the first sample of the event per pixel
12
13 # Fill the arrays
14 event_index = 20
15 reader.GetR1Event(event_index, waveforms, first_cell_ids)
16 # 'waveforms' array is now filled with entire event's waveform data
```

4.3.3 `TargetCalib`

To correct for the effects of the TARGET electronics on the waveforms, `TargetCalib` was built. I have led the development of this package since its early development. The calibrations performed by this library are detailed in Chapter 5. This package has also been adopted by SCT recently.

The main classes in the library include:

PedestalMaker Generates the *Pedestal* calibration file.

TfMaker Generates the *Transfer Function* calibration file.

Calibrator Applies the aforementioned calibration files to the waveform samples.

Mapping Handles the files containing the camera's pixel mapping, and provides an interface to the information. This class is necessary due to the non-intuitive mapping between physics pixel position, and order of pixel readout (Figure). Most commonly, this mapping is used for the plotting of camera images. The class is compatible with the mapping of any square-pixel telescope, and customisable to provide the mapping of the pixels in a single module, the mapping of the superpixels, the mapping of the modules, or the neighbours to a pixel/superpixel/module. This class will be deprecated once the central CTA database of telescope configurations exists.

figure showing the pixel positions, camera or module?

CameraConfiguration Provides an interface to certain camera-version dependant variables. Currently the variables that might change with camera-version (stored in the TIO file header) include number of storage cells, pixel mapping, and reference pulse shape. The correct version of the parameter is returned according to the camera-version provided, allowing for the automated processing of the data of different camera versions. This class will also be replaced by the central CTA database.

Efforts are being made to improve the `TargetCalib`'s (more specifically the `Calibrator` class's) efficiency in terms of both memory and processing time, as it will need to meet the CTA Requirements for *Online Analysis* (Chapter 3). It is possible that in the future there will be two separate `Calibrator` classes for the *Online* and *Offline Analyses* respectively.

4.4 Reduction Tools

Tools used to process the waveforms in order to either characterise the camera or progress down the data-level-chain (Figure 3.3) are often referred to as "reduction tools". Within the CHEC group we utilise Python for all of our waveform reduction. We made this choice due to its high popularity for data science and signal processing and its extensive library of statistical and numerical packages. The most important examples of these packages include:

NumPy[2] Enables the efficient processing of numerical data. This is accomplished using their powerful N-dimensional array object known as a `numpy.array`. At

[2] http://www.numpy.org/

the lowest level, a `numpy.array` is a contiguous block of memory much like a C array. However, NumPy defines many statistical methods which utilise optimised low-level C and Fortran operations to process the contained data in the most efficient way possible, often performing better than handwritten C or Fortran.

Different reduction packages may be designed with different purposes, but each can potentially import methods from another, which is especially possible when developing in Python. Many other CTA groups have also adopted Python for their waveform reduction software, but it is not a standard across CTA.

4.4.1 `ctapipe`

4.4.2 `CHECLabPy`

4.5 Science Tools

4.5.1 `GammaPy`

4.5.2 `CTOOLS`

5

Calibration

Contents

:

5.1 Plan

5.1.1 Topics

- Pedestal subtraction
- Transfer functions
- Gain Matching
- SPE
- Flat fielding
- Time correction
- Future
  - Live calibration

5.1.2 Questions

- TARGET architecture diagram, Wilkinson ADC
- How much detail about all the TF approaches do I go into?

Flow diagrams? See Cyril talk 18/07/06 camera calibration call

5.2 Introduction

In order to obtain meaningful and reliable results from the camera, a number of calibrations must be applied to the waveforms read. A primary objective of my DPhil is to investigate the most optimal and efficient approaches for these calibrations (in accordance with the CTA requirements described in Chapter 3), and to determine if additional calibrations are required.

The calibrations applied have evolved during the course of the prototyping of CHEC; the calibrations applied to CHEC using MAPMTs as the detector (CHEC-M) waveforms are not the same for CHEC using SiPMTs as the detector (CHEC-S). Additionally, the calibration applied for the on-sky pipeline can differ from the calibration used to obtain results such as the charge resolution.

When I joined the CHEC development, the calibration discussion was still in its infancy. Some approaches had been tested in a laboratory environment [10], but there had been little discussion on how exactly the calibrations could be applied efficiently in an analysis pipeline, where one might not be able to use the same detailed calibration due to limited resources (such as memory and time). A major contribution of my DPhil was to prototype the calibrations procedures, develop an approach for a calibration pipeline, write the software to perform such a pipeline, and finally assess the performance of the pipeline. This was an iterative procedure,

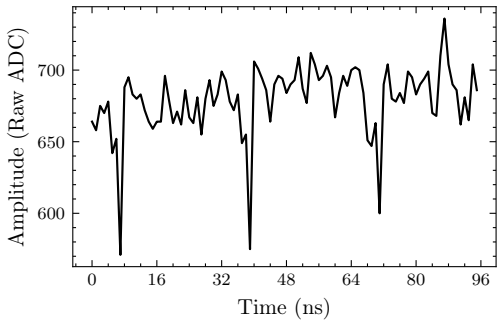

Figure 5.1: TARGET-C waveform as read out from CHEC-S, showing the electronic pedestal in the absence of any other input, before any calibration is applied.

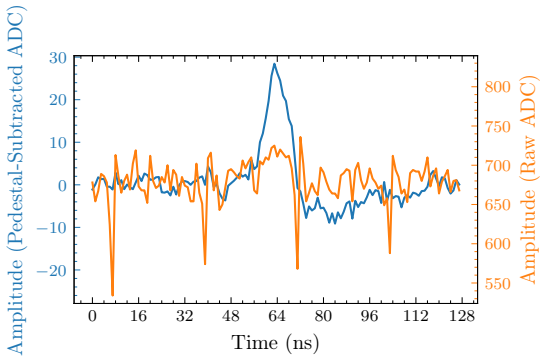

Figure 5.2: CHEC-S waveform containing a 5 p.e. pulse, before and after pedestal subtraction.

the development of which is still ongoing. However, a procedure now exists that allows us to obtain meaningful results from the waveform data, a capability that is of paramount importance in the commissioning of the camera.

In this chapter I will outline each of the calibration steps that are presently adopted for CHEC. They are introduced in the general order that they are applied, and split into the categories of TARGET ASIC, photosensor, and "other" calibrations.

5.3 TARGET Calibration

The calibrations described in this section relate to the TARGET module. As detailed in Chapter 2, the TARGET ASIC is responsible for the sampling, digitisation and readout of the waveform data. As a result there are two calibrations that are solely related to the TARGET ASIC: electronic pedestal subtraction and the linearity correction via the transfer function.

The functional block diagram of the TARGET ASIC in Figure 2.1 outlines the electronics responsible for the need of these calibrations, and should be used as a reference in the following descriptions.

As the calibrations in this section are very low-level, and related to CHEC's specific Front-End Electronics (FEE), they are handled by the TargetCalib library (Chapter 4).

5.3.1 Electronic Pedestal Subtraction

421.10046pt

The most important, but also the simplest, calibration to apply is the subtraction of the electronic pedestal. Each cell in the storage array of the ASIC is a unique

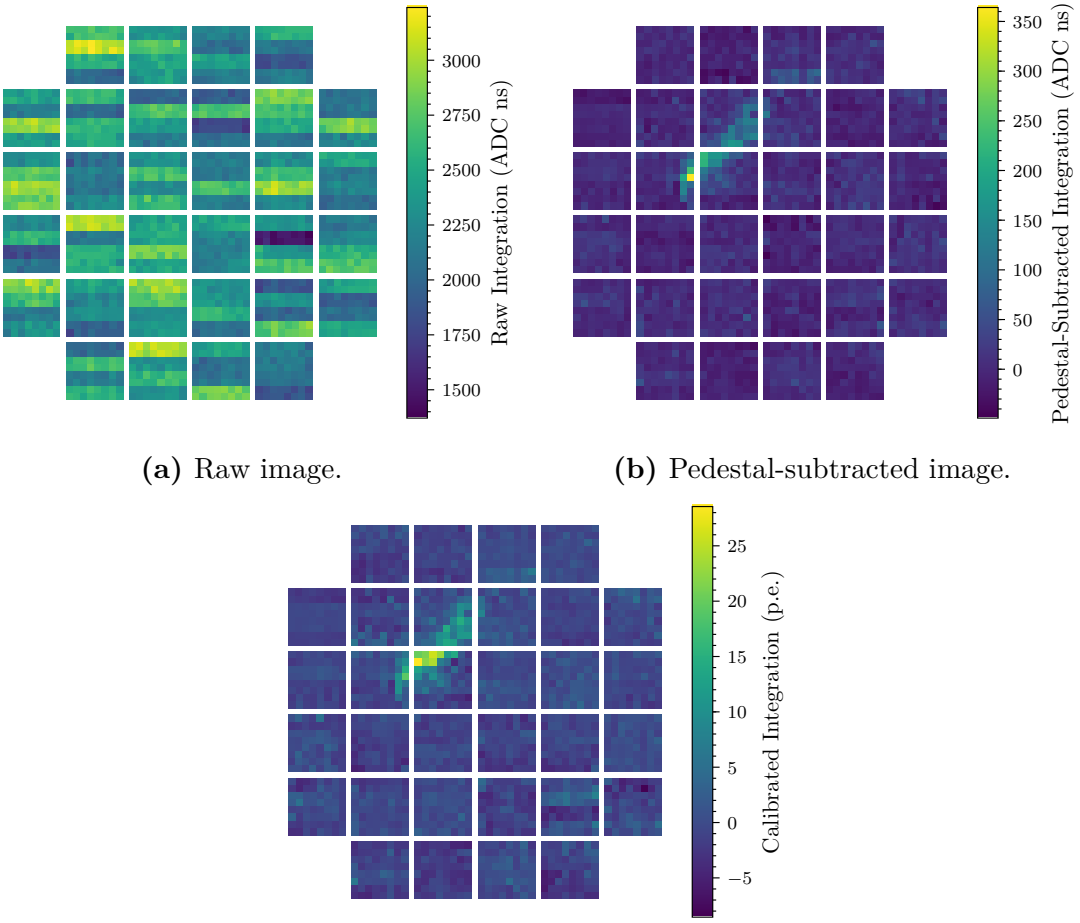

(a) Raw image.

(b) Pedestal-subtracted image.

(c) Final calibrated image.

Figure 5.3: The same image of a Cherenkov shower taken with CHEC-M, but at different stages of calibration. An integration window is chosen using the *Neighbour Peak Finding* technique (Chapter 6) on the p.e. calibrated waveforms. The same samples are then integrated for each of the calibration stages.

capacitor. For a specific input input pedestal voltage (Vped), each capacitor has its own resulting electronic pedestal value. As each sample of the waveform corresponds to a single storage cell, each sample therefore has a unique pedestal value to be subtracted. This is apparent in Figure 5.1 where the variation from sample-to-sample is very large. This variation is large enough that low-amplitude pulses (Figure 5.2) and low-amplitude Cherenkov images (Figure 5.3a) are undetectable in the camera. This variation in electronic pedestal is also apparent between pixels, and even more so between ASICs. As a result, the outlines of the ASICs are the dominating feature in camera images containing raw samples, such as Figure 5.3a. With the pedestal subtraction alone, the waveforms are transformed into a state of which a moderate amount of Cherenkov shower assessment can be performed, as demonstrated in Figure 5.3b.

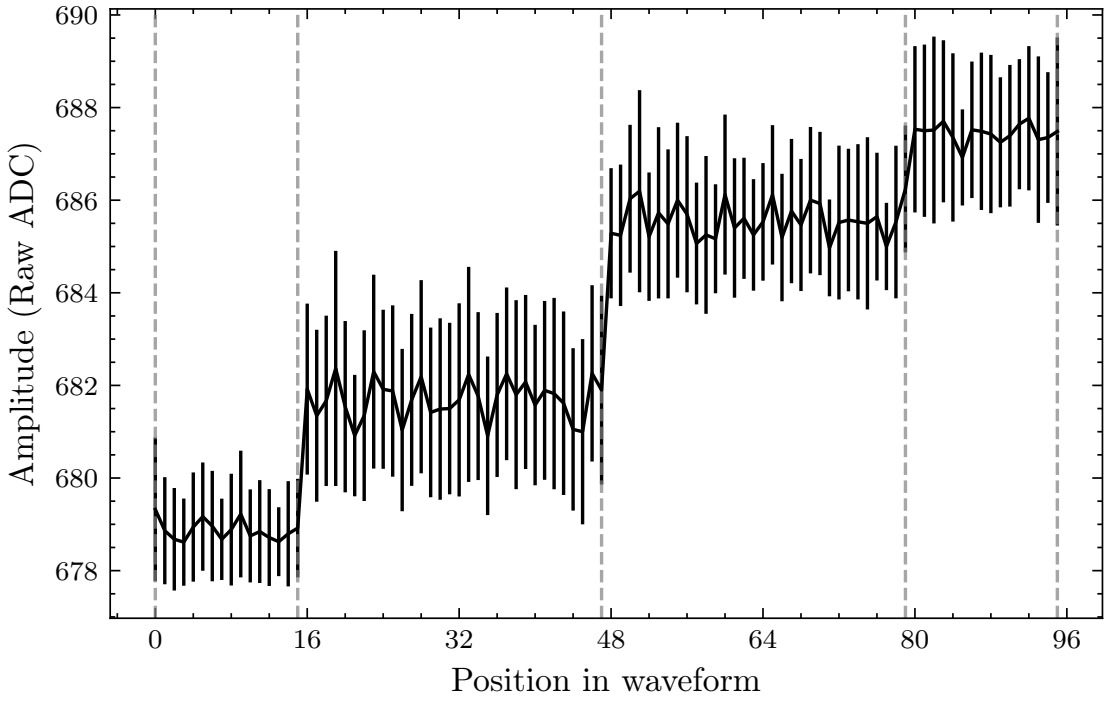

Figure 5.4: Average amplitude of the electronic pedestal for a single storage cell in a TARGET-C ASIC, at different positions in the waveform. Error bars indicate the standard deviation of the amplitudes. The grey dashed lines indicate the position of the block edges in the waveform for this cell. The average of the values inside each block segment equals the pedestal value stored in the lookup table for that cell, in each of those block positions.

There are $2^{14} = 16,384$ storage cells per channel (for CHEC-M, $2^{12} = 4096$ for CHEC-S), therefore naively it could be concluded that there are $32(Modules) * 64(Channels) * 16,384(Cells)$ pedestal values to keep record of. However, an additional characteristic of the TARGET ASIC is that the pedestal amplitude depends on the position in the waveform. This occurs as the blocks are not entirely decoupled; the discharge of one block affects adjacent blocks. This effect is apparent in Figure 5.4, where the pedestal amplitude of a single cell changes depending on the position of its parent block in the waveform. Consequently, an extra dimension of "position in waveform" needs to be considered in the waveform lookup table.

Make sure to mention about the difference in number of cells for checs in ch2

Generation

In order to perform the pedestal subtraction, one must first generate a lookup table of pedestal values. This can be easily obtained with a calibration run where the voltages across the photosensor are disabled, and forcing the camera to trigger (with either an external pulse generator, or internally via software) to obtain a large amount of waveform data. Typically around 30,000 events provide

enough samples for every storage cell, in every waveform position, to be hit at least 10 times. The samples are then collected as a running average with the dimensions $[Module, Channel, StartingBlock, Blockphase + Sample\_i]$, where the *StartingBlock* is the storage block that the first sample in the waveform belongs to (see Figure), *Blockphase* is the cell index within the storage block that the waveform begins on, and *Sample_i* is the index of each sample in the waveform. This is illustrated in Figure , where for these two readout windows shown, the pedestal running average `Pedestal[TM][CHANNEL][9][8:103]` and `Pedestal[TM][CHANNEL][8][12:107]` will be contributed to, respectively.

include figure, and edit to use bp 8 and 12

The TargetCalib library handles the pedestal lookup table generation, and stores it into a FITS file. A new pedestal file is typically generated at the start of each new dataset, as the dependencies on temperature and evolution with time are still being investigated.

Application

To apply the pedestal, the entry within the lookup table that corresponds to each sample is subtracted from the waveform. The result of the subtraction can be seen in Figures 5.2 & 5.3b.

Performance

The primary quantification of this calibration's performance is the standard deviation of electronic-pedestal samples that have had separately-created pedestal values subtracted from them. Figure 5.5 demonstrates the performance of the pedestal subtraction for a TARGET (version C) (TARGET C) channel, achieving a residual variation of 1.6 ADC (approximately 0.5 p.e.).

5.3.2 Transfer Function

The other calibration related to the digitisation and readout inside the TARGET ASIC is caused by the non-linearities in the storing and reading of charge to and from the storage cells. The components responsible for the need for this calibration are the sampling array, gain/buffer amps, and the Wilkinson Analogue-to-Digital Converters (ADCs), seen in Figure 2.1. The non-linearity of these components is propagated to the sample readout - a sample with twice the amplitude input into TARGET will have less than twice the amplitude when readout.

To correct for this non-linearity, a look-up table is generated to convert from the sample amplitude read-out (in ADC), to the input sample amplitude (in mV). This

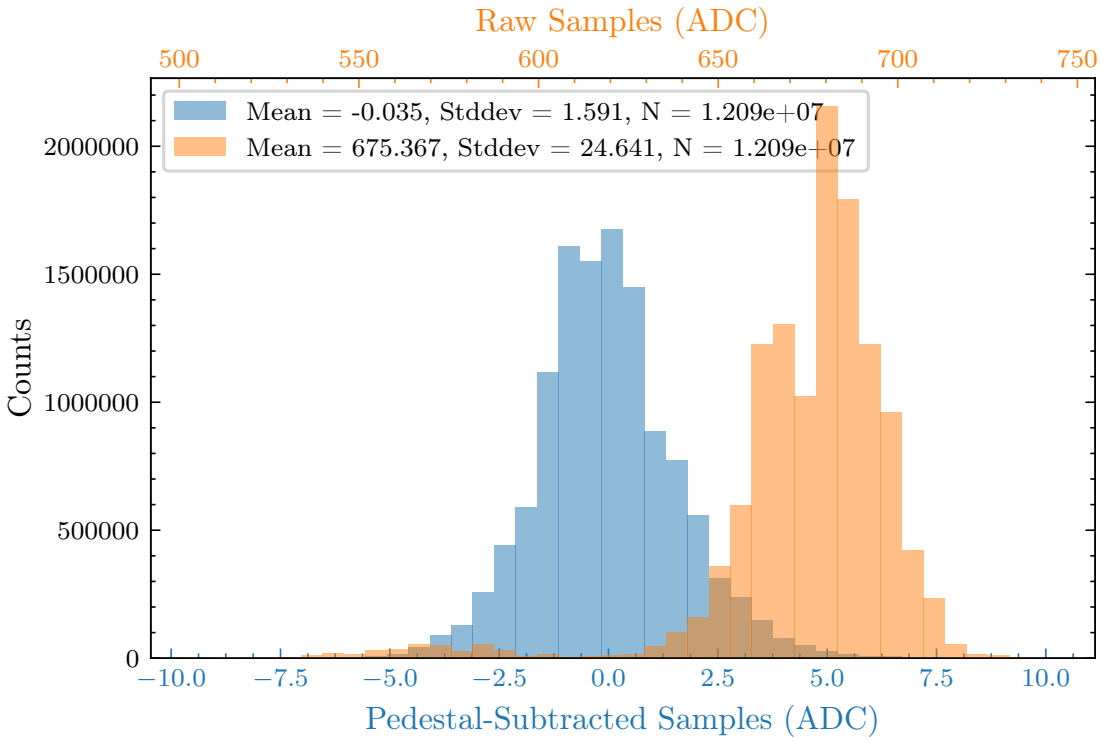

Figure 5.5: Spread of electronic-pedestal values before and after the pedestal subtraction for a single TARGET-C channel. The waveforms used to create the pedestal lookup table are separate to those used in these histograms.

look-up table is known as the Transfer Function. As one might expect, each sampling cell has its own linear response to correct for, and therefore a look-up table is typically required at-least per channel and per sampling cell, however a noticeably improved performance is observed by considering a Transfer Function per storage cell .

need to show this, maybe in TF Investigations appendix?

There are two forms of Transfer Function that have been considered for CHEC, distinguished by the type of input used to generate them. A Direct Current (DC) Transfer Function is created by applying a constant DC input of known voltage into the module, and iterating over the full dynamic range by varying the voltage. An Alternating Current (AC) Transfer Function is generated by inputting a pulse of a known amplitude with a shape expected from the photosensor, and iterating as with the DC approach. During previous investigations of the TARGET module, where sinusoidal signals were input into the module, a dependence on the signal frequency and input amplitude was observed that acts to further reduce the output amplitude [10][2]. The source of this dependence was deemed to be due to the amplifiers, which cannot slew fast enough to keep up with the input signal if the frequency and amplitude are large. Due to the use of a pulse to generate the AC Transfer Functions, the result inherently includes the correction required for the frequency that the pulses correspond to.

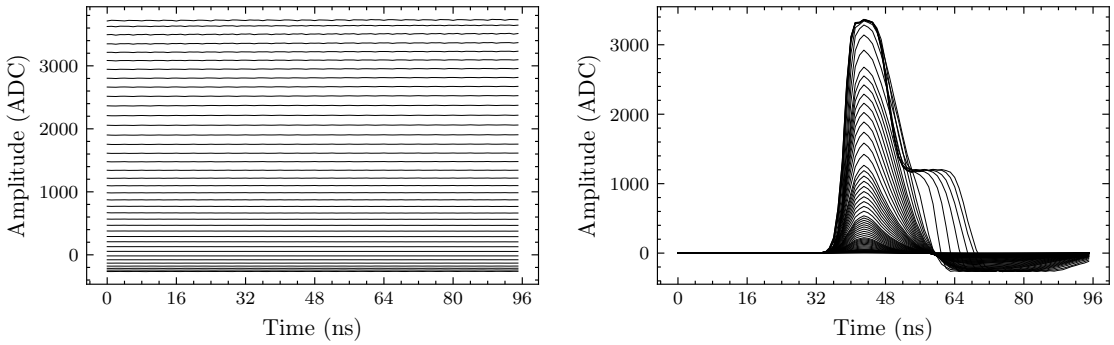

(a) DC Transfer Function input, measured with TARGET 5.

(b) AC Transfer Function input, measured with TARGET C.

Figure 5.6: Multiple average waveforms, increasing in amplitude. Each average contains 1000 waveforms from the same single channel. These waveforms cover the full dynamic range of the TARGET ASIC, and are used as inputs to generate the DC and AC Transfer Functions, respectively. The saturation behaviour of the TARGET C ASIC can be seen in the high amplitude waveforms in (b).

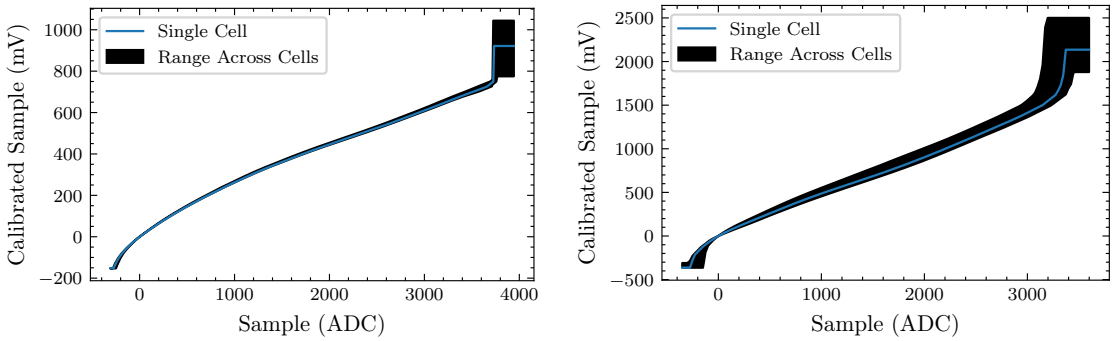

(a) DC Transfer Function lookup table, measured with TARGET 5. Contains 64 Transfer Functions, one for each Sampling Cell.

(b) AC Transfer Function lookup table, measured with TARGET C. Contains 4,096 Transfer Functions, one for each Storage Cell.

Figure 5.7: The Transfer Function lookup tables for a single channel.

Generation (DC Transfer Function)

During the commissioning of CHEC-M, a DC Transfer Function was used with no AC corrections. To generate this Transfer Function the internal input pedestal voltage (Vped) setting is used to apply a DC voltage offset of known amplitude. By repeating the process for Vped values from 500 mV to 1700 mV, in steps of 25 mV, the full dynamic range of the module is explored, covering the range -250 ADC to 3700 ADC (Figure **??**). The running averages of the ADC samples are grouped and monitored according to $[Module, Channel, Sampling\ Cell, Input\ Amplitude]$, utilising every sample in the waveform. Around 1,000 events are required to

provide sufficient statistics.

The second step in the generation is to linearly interpolate the running averages at the ADC points defined by the user. This provides a lookup table of mV values with dimensions $[Module, Channel, Sampling\ Cell, ADC\ Value]$ that can be used to provide a calibrated value for a measured ADC value. The lookup table for a single channel is illustrated in Figure 5.7a. This table is saved to a FITS file, ready for application.

Generation (AC Transfer Function)

As the ability to internally set a DC voltage with a known amplitude via the Vped was removed in TARGET C (see 2) , and the ability to input a DC voltage externally is prohibited by the AC coupling of the module , the decision was made to transition to an AC Transfer Function that uses the expected pulse shape as an input. This approach therefore corrects for the AC effect with the appropriate frequency.

more precise ref, and remember to mention this change

remember to introduce ac coupling

The full dynamic range is once again probed, by injecting pulses of varying amplitude. In order to extract the values that correspond to negative amplitudes in this method, the amplitude of the input undershoot is also monitored. Only the samples that correspond to the maximum of the input pulse (and minimum of the undershoot) has a "true" amplitude of the input amplitude. Therefore to extract the correct samples, each waveform is fitted with two Landau functions, a fair approximation to the pulse shape (Figure). Consequently, only two samples are extracted per waveform, requiring a much larger population of events (~200,000) in order to generate a reliable running average grouped according to $[Module, Channel, StorageCell, InputAmplitude]$. It is important to note that a Transfer Function per storage cell was adopted for TARGET C, as it was found to significantly improve the residuals (see Appendix **??** for further discussion).

figure showing the fit

The second step in the generation is identical to the DC Transfer Function. The resulting lookup table for a single channel can be seen in Figure 5.7b.

Application

Irrespective of the Transfer Function type, they are stored in a format which enables them to be applied identically. When calibrating an ADC sample, the relevant lookup table is obtained according to the channel and cell of the sample, and is linearly interpolated to provide the calibrated mV value for the specified ADC value.

Performance

Due to its complexity and variety of approaches, the Transfer Function is still one of the most actively discussed aspects of the CHEC calibration, and holds the highest potential for improvements among the different calibrations. Some possibilities for improvement include:

- An improved sample extraction method for the AC Transfer Function Waveform,
- Possibilities for a DC approach for TARGET C,
- Returning to the approach described in earlier TARGET studies where the pedestal is included inside the Transfer Function [2],
- Alternatives to linear interpolation, such as Piecewise Cubic Hermite Interpolating Polynomial (PCHIP),
- Exchanging the lookup table for a parametrised regression characterisation of the Transfer Function (such as a high-order polynomial),
- Decision between "per storage cell" or "per sampling cell",
- Inclusion of temperature corrections.

Appendix **??** provides some insight into the current progression in these active investigations.

Assessing the performance of the Transfer Functions is a more complicated task than for the pedestals. This is largely because instead of a comparison to a null signal, we are instead comparing to an input amplitude which contains its own uncertainty, and could potentially be incorrect. So while the performance results may indicate that the residuals of the Transfer Function may be small, this does not necessarily mean the calibration is accurate. Therefore the most decisive performance indicator should be one that provides an independent measurement on the “correct” amplitude. The most obvious scheme fitting this requirement is the charge resolution, described in Chapter 3, the results of which are also explored in Appendix **??**.

5.4 Photosensor Calibration

The other primary component in the detector chain that requires calibration is the photosensor itself. As photosensors are a much more common instrument used in a variety of experiments, the calibration procedures required are already well known in the academic community. It is therefore mostly a simple case of adapting existing approaches to fit our requirements.

The typical procedure in Cherenkov camera waveform analysis includes extracting the signal charge from the waveform of each pixel. This procedure, and the different methods to achieve it, is described in Chapter 6. The value extracted is typically in digitisation counts or units of voltage, multiplied by time if the charge extraction is an integral over the waveform. For example, the units of the extracted charge from CHEC-S using the *Cross-Correlation* method is $mVns$. Once extracted, this charge must be corrected for the relative efficiency of its pixel compared to the mean of the camera in order to achieve a uniform response ("flat-fielding"), and then converted into a counting unit that is common among the telescopes in the array (such as photons or photoelectrons), thereby simplifying the processing of array data [11]. This procedure is characterised in the equation:

$$I_i = \frac{A_{Q_i} - A_{0i}}{\gamma_Q} \times \gamma_{FFi}, \tag{5.4.0.1}$$

where

- A_{Q_i} is the charge extracted in units of $mVns$ for pixel i, proportional to the number of photoelectrons,
- A_{0i} is the baseline in the absence of a signal for pixel i. It should be obtained using the same charge extraction approach used for the signal,
- γ_Q is the nominal conversion value from $mVns$ to photoelectrons/photons for the entire camera,
- γ_{FFi} is the flat-field coefficient for the pixel i,
- and I_i is the resulting calibrated signal in photoelectrons/photons.

In the final calibration design of CTA, A_{0i} is intended to be supplied by the telescope alongside the waveforms at regular intervals. The regular updating of this value ensures that any changes to the baseline due to NSB or temperature variations (which can also increase DCR) are accounted for. However, this parameter is set to zero for the content of this thesis, and is not investigated. Instead, a less effective

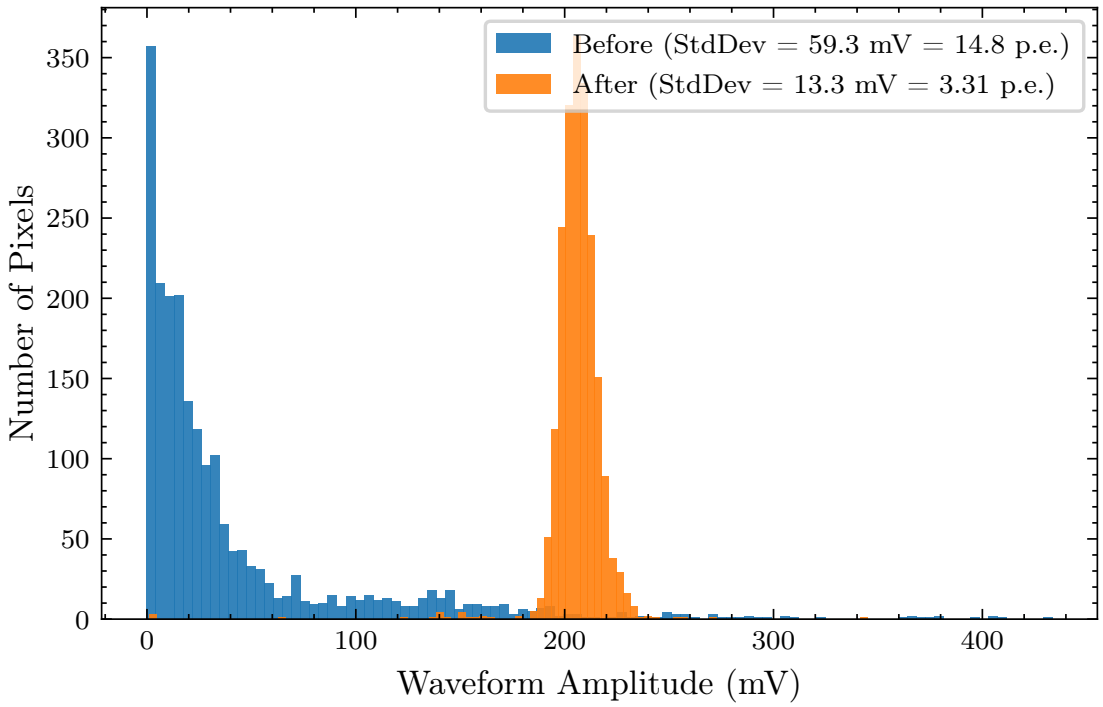

Figure 5.8: Comparison between the spread in the average signal amplitude per pixel before and after gain matching, for a dataset with approximately 50 p.e. average illumination. Every pixel in the camera is included.

but simpler baseline subtraction is performed by monitoring the running average of the first 16 samples of the past 50 waveforms for each pixel. This running average is subtracted from each waveform before charge extraction. The remainder of this section will describe how to obtain the other calibration values, γ_Q and γ_{FF_i}, and the other procedures related to the photosensor calibration.

5.4.1 Gain Matching

The flat-field coefficients, γ_{FF_i}, provide an offline compensation for a variety of photosensor parameters which alter the signal response in the waveform, described in Tables x&y. However, as seen in the table, many of these parameters have a dependence on the voltages across the photosensor, which is a controllable value. With the CHEC-M MAPMTs it is only possible to change the voltage value for an entire module, whereas with the CHEC-S SiPMTs the voltages can be configured per superpixel (group of four pixels). Therefore, voltage values can be selected before data-taking that result in a more uniform signal response across the photosensor. This is referred as "Gain Matching", however the name is slightly misleading, as it is the signal that is being matched, not the gain. It is performed by specifying

create table in mechanics chapter that list each parameter for the photosensor, with descriptions and specify if it changes with voltage, temperature, and how it affects signal

mention superpixels in ch3

the amplitude (in mV) that every pixel should be matched to, and then performing the following iterative procedure:

1. The camera is uniformly illuminated with approximately 50 p.e..
2. The waveforms are readout, calibrated, and averaged per superpixel/module (excluding any dead pixels).
3. The peak amplitudes of the average waveforms are extracted.
4. Each module/superpixel is categorised as being above or below the requested amplitude
5. Depending on their category, voltage setting is increased or reduced by steps of 5 (in units of DAC value), such that it increments closer to the requested amplitude. If the amplitude has been overstepped in the previous measurement, a smaller step value is used. The minimum DAC step value available is 1, which corresponds to $\frac{10}{256}$ V. If the amplitude is not responding to changes in voltage, the pixel is classified as "dead", and excluded from the average waveforms.
6. The new voltage settings are applied and the process is repeated.

In the future, this iterative technique will be replaced with a set of lookup tables for different requested amplitudes. These lookup tables will contain the final voltage settings resulting from this iterative technique. Additionally in the future, the requested signal will not be specified in terms of peak amplitude, but in terms of the *Cross Correlation* charge extraction approach. The improvement in signal response for CHEC-S as a result of the gain matching is shown in Figure 5.8, where a response spread reduction of 22% is achieved.

Tables x&yalso show a dependence on temperature for some of the photosensor parameters. The additional benefit of the gain matching is these temperature dependences can also be accounted for, by using the monitored temperature value per module and a lookup table of the appropriate corrections to the voltages, such that a constant signal response is kept across the camera. This particular in-situ calibration has not yet been implemented, but is intended for the future.

update

plot with gain vs temperature? maybe some initial results from Yuki

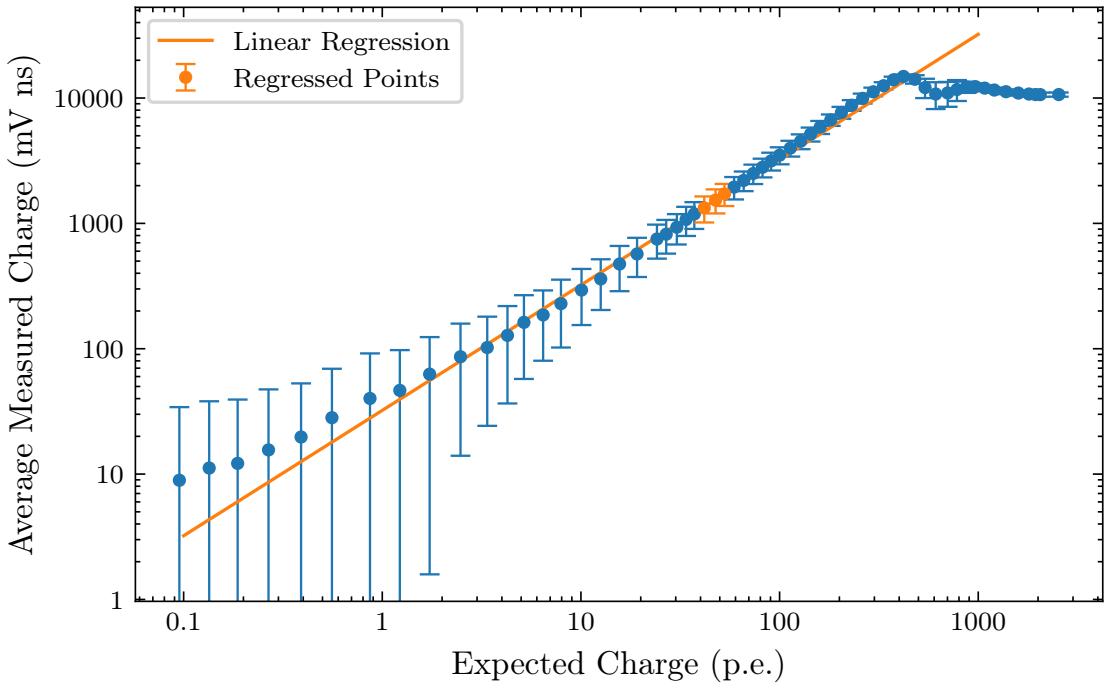

Figure 5.9: The average measured charge per illumination for a single pixel. The orange points are used for a linear regression through the origin in order to determine the flat-field coefficients for each pixel.

5.4.2 SPE Fitting

Due to the photon-counting nature of MAPMTs and SiPMTs, when the signal extracted from a pixel, illuminated with a low light-level (~1 p.e.), is accumulated into a histogram, the resulting spectra (Figure) show peaks at regular intervals corresponding to the baseline (zeroth peak), 1 p.e. (first peak), 2 p.e. (second peak), etc. These spectra are referred to as "Single Photo-Electron (SPE) Spectra". The physical processes that result in these spectra are well understood for MAPMTs and SiPMTs, and therefore analytical formulae exist describing the spectra. When these formulae are fit to the histogram, they can be used to extract certain parameters of the photosensor, including the average incident illumination λ, in units of photoelectrons. As λ provides an absolute illumination value, it allows for the full calibration of expected charge for each filter-wheel position, for each pixel (Section **??**). This is the first step required in obtaining the flat-field coefficients. For more details on this fitting procedure, and the formulae used to describe the SPE spectra, refer to Appendix **??**.

figure of both checm and checs spectra

check consistency in spelling

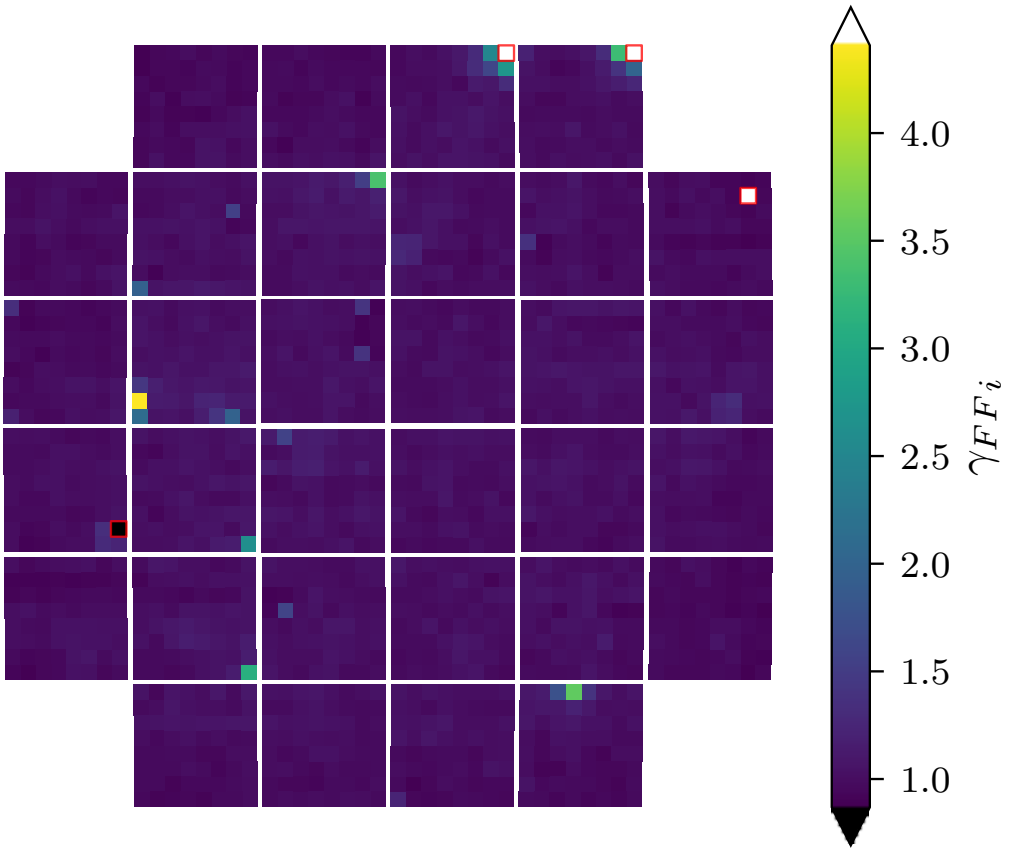

Figure 5.10: Camera image of the flat-field coefficient value, γ_{FFi}, per pixel. Pixels that have been designated "dead" or misbehaving are outlined in red, and exist beyond the colour-scale range.

5.4.3 Flat-Field Coefficients

Once the "expected charge" dependence on filter-wheel position/transmission is characterised (Section **??**), we can calculate the coefficients, γ_{Mi}, required to convert the average extracted charge (in $mVns$) into the charge we expect (in photoelectrons/photons). The application of these coefficients to the extracted charge has two effects:

- The signal response between pixels is homogenised - the same average amount of charge will be extracted for any pixel illuminated with an average of N photons.
- The signal response is converted into the common telescope-array units of photoelectrons or photons.

Therefore:

$$\gamma_{Mi} = \frac{\gamma_Q}{\gamma_{FFi}}. \tag{5.4.3.1}$$

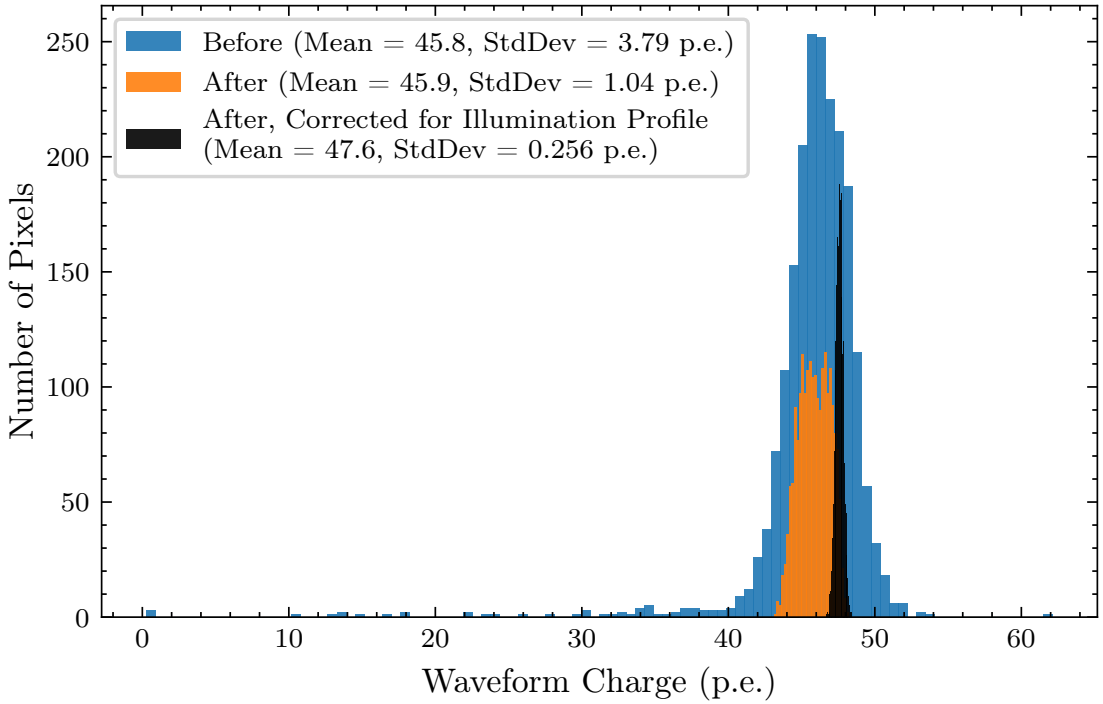

Figure 5.11: Comparison between the spread in the average signal amplitude per pixel before (blue) and after (orange) the flat-fielding calibration. The charges are extracted from a dataset where a theoretical pixel located at the centre of the camera would be expected to have a charge of 47.7 p.e.. The black histogram contains the charges after the difference in the illumination profile (Section 2.8.2) between the pixels is considered, i.e. they contain the charge that would be measured if every pixel was located at the camera centre. Every pixel in the camera is included in the histograms.

To obtain γ_{Mi} per pixel i in the lab, datasets with around 50 p.e. expected charge per pixel are produced. For each pixel, the average extracted charge (in $mVns$) is linearly regressed, while forcing the fit through the origin. This regression is shown for a single pixel in Figure 5.9. The resulting gradient of the regression is equal to γ_{Mi}, which can now be combined with Equations 5.4.0.1 & 5.4.3.1 to obtain the calibrated extracted charge. The value of γ_Q obtained for CHEC-S is 32.56 mVns/p.e., and the spread of γ_{FF} across the camera is shown in Figure 5.10. The resulting residual spread in signal response between pixels at an average camera illumination of 47.7 p.e. is shown in Figure 5.11. The final variation in signal response between pixels at this illumination is 0.5% . The variation in signal responses at other illuminations is shown in Figure .

update when using the lab illumination profile

add figure

As the flat-field coefficients have been calculated in a manner in which they are unfolded from the illumination profile (by calculating the expected charge individually for each pixel), they are applicable to any environment the camera is used in. Any deviations that are observed in the signal between pixels are then

due to the illumination profile present in the environment, and not due to the characteristics of the photosensor. Once on telescope, the flat-field coefficients are intended to be routinely updated using the reflection of the LED flashers (Section **??**) in the secondary mirror. This will calibration will require an updated illumination profile in order to be performed.

5.4.4 Dead Pixels

It can be seen from Figure 5.10 that some of the photosensor pixels contain either no signal or an odd signal, resulting in an extreme flat-field coefficient. This is likely due to damage to the pixel during handling, or due to water ingress. However, the 4 pixels constitute to 0.2% of the camera, therefore the camera is still well within the **B-TEL-1295 Pixel Availability** CTA requirement. These pixels are excluded from any calculations involving multiple pixels, including the expected-charge calibration and the camera charge-resolution.

5.5 Saturation Recovery

As evident in Figure 5.9, high illumination (greater than ~200 p.e.) measurements are affected by saturation of the detector. The saturation seen is due to the TARGET ASIC, which saturates before the photosensor itself. However, while the height of the pulse will increase no further, the excess charge causes the pulse to extend further (Figure 5.6b). Therefore it is possible to perform a simple correction for the saturation recovery by utilising this waveform behaviour. A simple attempt at saturation recovery is shown in Figure , where the waveform is integrated in a window that starts just before the pulse maximum, and extends to the end of the waveform. This results in an extracted charge that continues to increase with illumination, apart in the region immediately after saturation. More investigation is required for this calibration.

add figure

5.6 Timing Corrections

Due to the routing of the electronics in the front-end, the electrical signal path is slightly different per channel, causing a small difference in apparent arrival of the pulse in the waveform. The relative arrival time per pixel can be seen in Figure .

Not only does this need to be taken into consideration when investigating the timing performance, it also can have a significant impact on the charge extraction, which typically relies on other pixels (neighbouring or entire camera, see Chapter 6)

add camera image showing relative time

sharing a compatible pulse time. The effect of a 1 ns incorrectly extracted charge (when the peak finding is done using the waveforms from all pixels) can have the impact on the charge resolution shown in Figure . Discussions are ongoing on how to best include the timing corrections in the charge extraction.

show impact of an incorrect time extraction on charge resolution, maybe of just TM?

5.7 Future

During the long development of CHEC, the calibration procedure has evolved a lot, and multiple iterations have occurred to either:

- accommodate the changes required in the upgrades of hardware (such as from TARGET (version 5) (TARGET 5) to TARGET C),
- simplify the calibration to save on computing resources,
- or account for additional factors, thereby improving the calibration (such as the AC contribution to the Transfer Functions).

Therefore, while each iteration improves in one aspect, it may be at the expense of the others. As a result, the TARGET calibration procedure described in this chapter appears quite complicated compared to the approaches detailed in [10] and [2]. The primary next step in the calibration development for CHEC is therefore to review the procedure used, with the aim to produce an approach that is simpler, includes aspects such as temperature dependence, and meets the requirements and processing rates required by CTA.

6

Pipeline Reduction

Contents

:

6.1 Plan

6.1.1 Topics

- Charge Extraction Methods
- Image cleaning
- Shower reconstruction
  - Hillas
  - Impact
  - model
  - Neural Nets
  - ++
- Energy Reconstruction
- Direction Reconstruction

6.1.2 Questions

- ?

6.2 Introduction

Following the low-level calibration detailed in 5, the waveforms should no longer require any further corrections unique to the electronics they were produced with. The waveforms from CHEC should now be in such a state that they can be processed in the same way as the waveforms from other cameras. This chapter describes the reduction performed on the waveforms in order to extract the Cherenkov shower information. With regards to the CTA data levels (Figure), this concerns the steps from DL0 to DL2 .

figure with data levels in ch3

double check dl

These reduction methods have been a primary component of Imaging Atmospheric Cherenkov Telescope (IACT) analysis since the beginning of the field, therefore much thought and development has previously been performed on these techniques. As CTA is a large consortium that essentially consists of the worldwide IACT community, the developers of the reduction approaches for previous IACTs have brought them forward to CTA. However, due to:

(a) CTA is to consist of the most advanced IACTs to date, with higher shower imaging resolution and multiplicity than has previously been available

(b) the capabilities of digital signal processing has significantly increased in the past decade

The opportunity for more advanced and more successful algorithms exist within CTA. Some effort has already been made in this direction, but it is an aspect that is expected to constantly evolve and improve during the lifetime of CTA. In this chapter I will attempt to provide a broad overview of the existing and in-development reduction techniques, with an especial focus on charge extraction approaches due to my involvement in developing them.

improve sentence

6.3 Charge Extraction Methods

The most low-level reduction stage is the extraction of information from the calibrated waveforms provided by each camera individually. This procedure is very generic, allowing for the utilisation of common signal processing techniques that are not unique to Cherenkov shower analysis. The goal is to extract as much information from the pulse created by the Cherenkov shower light, while simultaneously limiting the amount of noise introduced from factors such as NSB . Two quantities are extracted in this stage: the signal charge in each pixel (the sums of which is a measure of the energy within the shower), and the signal arrival time per pixel.

talk about all the contributing factors (noise etc.) to waveforms in ch2

The total signal charge in a pixel, i.e. the total number of photo-electrons released from the PMT's photocathode, is proportional to the total area below the pulse corresponding to the Cherenkov photons. If the waveforms were completely free of noise, and the readout window was large enough to capture the full Cherenkov signal, a simple integration of the entire readout would be a satisfactory approach for obtaining the signal charge. However, as we do not have the luxury of perfect waveforms, more complex methods are designed. Charge extraction algorithms typically consist of two aspects: how the signal pulse is found, and how the pulse is integrated.

6.3.1 Peak Finding

Two factors must be considered when finding the signal pulse of a Cherenkov shower. Firstly, the majority of camera pixels will not contain any Cherenkov signal while still containing noise. Secondly, due to the nature of Cherenkov showers (Chapter), those pixels with Cherenkov signal will have different arrival times due to the time evolution of the Cherenkov image . This time gradient across the image is especially apparent for bright showers at a large core distance from the telescope. The most successful peak finding technique is the one that best accounts for those two factors. Some simple techniques used to define a peak time from a waveform include:

reference where the time gradient of Cherenkov showers are described

figure of peak time?

- **Local Peak Finding**: Each waveform is treated independently from the other. The maximum point in the waveform is treated as the peak/arrival time. This approach is intrinsically biased to assume every waveform contains a signal; therefore, in the absence of a Cherenkov signal, the largest noise pulse will be extracted, resulting in a higher total charge than should be obtained.

- **Global Peak Finding**: The waveform from every pixel is combined into an average, from which the maximum point is treated as the peak time for every pixel. This technique is only useful if a large portion of the camera is simultaneously illuminated, such as by a laser in the case of lab commissioning and calibration runs.

- **Neighbour Peak Finding**: The waveforms from the neighbouring pixels are combined into an average, from which the maximum point is treated as the peak time for the pixel-of-interest. This technique is often preferred for Cherenkov images as it has a reduced charge bias (especially if the pixel-of-interest's waveform is not included in the average); pixels with Cherenkov signal typically have neighbours that also contain Cherenkov signal at a correlated time, while the neighbours of empty pixels only contain noise, and therefore a random peak time is extracted.

- **Fixed Peak Value**: Due to a reliable definition of the camera trigger and subsequent electronic chain, the position of the pulse in the waveform could consistently be known a-priori, allowing for a fixed peak time. However, this method requires a larger integration window size in order to capture the full pulse in the tail of the Cherenkov shower, which occur at a later time than the initial photons which trigger the camera, therefore resulting in a larger noise included in the signal. However, this technique usually contains the least bias, as no signal is assumed to exist.

A more complex peak finding technique is the *Gradient Peak Finding* approach. This approach was designed for the VERITAS telescope [12][1][13], but is applicable to any IACT telescope with the ability of a dynamically choosing an integration window. *Gradient Peak Finding* is a two-pass approach where the time-gradient of the Cherenkov signal across the camera's focal plane is obtained by first extracting the signal using one of the other methods, and then cleaning and parameterising the image using simple techniques described later in this chapter. This time-gradient can then be used to assume a peak time based on camera pixel position. This

method provides a more unbiased estimation of the peak time of the signal at the expense of simplicity.

more verbose description from [1]

These peak finding methods have been described in relation to the maximum of the signal pulse, however they may instead use other characteristic positions of the pulse, such as the half-maximum time on the rising edge, or the centre of gravity of the pulse. Additionally, more advanced peak finding techniques may up-sample (possibly by zero-padding in the frequency domain via a Fourier transform) or interpolate the signal to obtain a more precise peak time [1][13], or even apply low-pass filters in order to remove low frequency baseline noise. The peak finding should be done in conjunction with any timing corrections () that may be required.

reference timing calibration section

maybe derive gradient here, and cross-correlation next, then each subsection has the full description of at least one complex algorithm

6.3.2 Integration

Once the peak time has been obtained, the simplest approach to extract the signal is to define an integration window centred about this time. The size of the window needs to be large enough to capture sufficient signal from the pulse, but small enough that not too much noise (NSB, dark counts, afterpulsing) is included within the window, thereby maximising the signal-to-noise. Additionally, the camera's pulse shape may not be symmetric, so a better signal-to-noise may be achieved by shifting the window a few samples with respect to the peak time. Typically, an integration window size on the order of ∼10 ns is used, with a shift of ∼3 ns. .

update values based on results

Beyond the simple "boxcar" integrator method (where every sample integrated has a weight of 1), other more advanced strategies may define their own alternative approach to extract the charge. One example is the fitting of the signal pulse, wither with an analytical description of the expected pulse, or with a more unconstrained description such as a cubic spline. A second complex approach is the use of digital filters, which can be used in combination with knowledge of the pulse shape to robustly extract the signal even in the presence of high noise. Such a technique has been designed and adopted for GCT, referred to as the *Cross-Correlation* method. Due to its adoption and sophistication, it is described here in more detail.

figures demonstrating the different peak finding

Cross-correlation is a common signal processing technique used as a measure of the similarity between two signals as a function of the displacement in time applied to one of the signals. Given a continuous function $f(t)$ defined between $0 \leq t \leq T$ and a second continuous function $g(t)$, the cross-correlation between the two functions $(f \star g)$ is defined as

$$(f \star g)(\tau) = \int_0^T \overline{f}(t) g(t+\tau) dt, \tag{6.3.2.1}$$

where $\overline{f}(t)$ is the complex conjugate of $f(t)$ and τ is the time displacement (also referred to as the "lag") between the two functions [14]. In descriptive terms, by varying τ, $g(t+\tau)$ will slide past $f(t)$. The cross-correlation for a value of τ_1 is then the integral across t of the product between $f(t)$ and $g(t+\tau_1)$. For a discreet function that is real-valued, such as a sampled waveform, Equation 6.3.2.1 can instead be defined as

$$(f \star g)[n] = \sum_{m=0}^{N} f[m]g[m+n], \tag{6.3.2.2}$$

where N is the total number of samples in the waveform and m is the sample displacement.

An illustration of the *cross-correlation* approach being applied on a CHEC-S waveform is shown in Figure . The peaks in the cross-correlation result correspond to the displacements where the signals match best, and the values of the peaks correspond to an weighted integral of the entire waveform. Therefore, through utilising a template of the expected pulse shape in the absence of noise (hereafter referred to as the "reference pulse"):

figure showing the cross-correlation at a few different times, and the different stages, 3 axes, maybe for a low illumination? mention I implemented 6.3.2.2 in Python

- the individual pulses in the waveform are emphasised against other background contributions, improving the ability to find the signal pulse (using the same methods detailed in section 6.3.1)

- the charge contribution from the signal pulse is accentuated, while the noise contributions are diminished

The reference pulse we use for the cross-correlation is an obtained via probing the input analogue signal on the TARGET module and averaged on an oscilloscope. It is then normalised such that cross-correlation between it, and the reference pulse normalised to have an integral of 1, has a maximum value of 1. This normalisation ensures that the cross-correlation result is in units of $mV * ns$, and allows an easy conversion into mV for "peak-height" investigations. An optimised implementation of cross-correlation exists in `scipy.ndimage.correlate1d` [15], where the waveforms for every pixel are processed in parallel.

6.3.3 Adopted approaches

Some examples of approaches adopted by other telescopes are outlined below.

MAGIC

Members of the MAGIC telescope performed a study comparing the techniques proposed for their signal reconstruction. In [16] they compare four approaches: *fixed-window*, *sliding-window* with amplitude-weighted time, *cubic spline fit* with integral or amplitude extraction, and *digital filter*. It is concluded the digital filter, which relies on knowledge of the signal shape to minimise the noise contributions, provides a charge reconstruction with acceptable bias and minimal variance, while remaining stable in the occurrence of small variations in pulse shape and position.

VERITAS

Similar to the aforementioned study for the MAGIC telescope, a comparison of charge extraction approaches was performed for VERITAS [12][1][13]. Specifically, the extraction methods compared include a *simple-window* using a-priori knowledge of the Cherenkov pulse time in the trace, a *dynamic-window* which slides across the trace to find the Cherenkov pulse, a *trace-fit* evaluator with fits the trace with two exponential functions which respectively describe the rise and fall time of the pulse, a *matched-filter* which "uses a digital filter based on the assumed shape of the FADC pulse to integrate the charge" [13], and finally an implementation of the *Gradient Peak Finding* approach described earlier in the chapter . At first glance, some of these approaches bear resemblance to those used by MAGIC, however there are slight differences:

should I move gradient peak finding to later, alongside the cross correlation method, as it has a nice analytical section from [1]

- in the VERITAS pulse fitting technique, an attempt to describe the pulse analytically was made whereas the MAGIC approach used a more loosely defined spline
- the filter used by VERITAS is a cross-correlation in Fourier space, whereas the filter used by MAGIC is generated using their knowledge of the noise auto-correlation matrix

Either as a result of these differences, or due to the difference in the instruments themselves, the *matched-filter* appears to result in a worse reconstruction than one would expect from the conclusion reached by MAGIC. One might justify that this degradation of signal extraction with the *matched-filter* for higher amplitudes is due to a change in pulse shape at higher amplitudes, thereby requiring a different "assumed FADC pulse shape", but it is not clear if that is what is occurring here. These studies conclude that the *matched-filter* "holds promise" for reconstructing low charges, whereas while the *trace-fit* performs extremely poor for the low charges (as expected), it performs the best for amplitudes > 4 photoelectrons [13].

Garret: However, a thorough investigation of this particular reconstruction is beyond the scope of this work

H.E.S.S.

The standard mode of charge extraction for the High Energy Stereoscopic System (H.E.S.S.) telescopes is to integrate N samples with respect to a fixed, but regularly verified, signal time [11]. H.E.S.S. camera electronics underwent an upgrade in 2015/2016, subsequently allowing for the update of the standard extraction mode to also output time-of-maximum and time-over-threshold, and also allowed for full sample readout enabling the utilisation of more complex charge extraction techniques [17][18].

FlashCam

The FlashCam Medium Size Telescope (MST) proposed for CTA utilises a custom digital filter approach in which the 4 ns-spaced samples are up-sampled and deconvolved, resulting in an approximately Gaussian pulse with a 9 ns FWHM. In the linear (non-saturated) regime, the peak of this Gaussian is directly proportional to the signal charge. need reference

ASTRI

Contrary to the other techniques described in this section, ASTRI

6.3.4 Performance Assessment

Deciding on which charge extraction method to use is not trivial - as shown in the above discussion, different cameras may perform better with different algorithms. This is anticipated in *ctapipe* (4), where different ChargeExtractors can easily be selected at runtime depending on the camera source.

6.4 Image Cleaning

6.4.1 Tailcut Cleaning

6.4.2 Wavelets

6.5 Shower Parameterisation

6.5.1 Hillas

6.5.2 Model and Model++

6.5.3 ImPACT

6.5.4 Neural Nets

6.6 γ-Hadron Separation

6.7 Energy Reconstruction

6.8 Direction Reconstruction

advanced techniques that don't fit into these categories, machine learning, photon counting

7

Camera Performance

Contents

:

7.1 Plan

7.1.1 Topics

- Charge Resolution
- TF Investigations
- Different NSB
- MC Validation
- MC Performance

7.1.2 Questions

- What other criteria?
  - Trigger performance - even though I haven't contributed

7.2 Introduction

7.3 Pulse Shape

7.4 Timing Characteristics

7.5 MC Validation

big diff between MC and the lab is the potential cross talk in the electronics and the effect e.g. of ground bounce - difference in full camera illumination

7.6 Charge Resolution

Justification of the lab chargeres using equation with ENF

Remember to talk about how the MC charge resolution provides us insight into performance with perfect Transfer Functions

7.7 Conclusion

8

On-Sky Pipeline

Contents

:

8.1 Plan

8.1.1 Topics

- Decided upon reduction methods
- Potentially different than for performance chapter
- CHEC-M campaign
- MC CHEC-S
- Future observations
- Jupiter observations (Beyond cherenkov?)

8.1.2 Questions

- ?

9 Summary

References

[1] Peter Cogan and Sullivan Supervised by John Quinn. "Nanosecond Sampling of Atmospheric Cherenkov Radiation Applied to TeV Gamma-Ray Observations of Blazars with VERITAS". In: December (2006).

[2] A. Albert et al. "TARGET 5: A new multi-channel digitizer with triggering capabilities for gamma-ray atmospheric Cherenkov telescopes". In: *Astroparticle Physics* 92 (2017), pp. 49–61. arXiv: 1607.02443. URL: http://linkinghub.elsevier.com/retrieve/pii/S0927650517301524.

[3] Francesco Dazzi et al. *CTA Architecture*. Internal Document (V1.0). CTA Observatory, 2018.

[4] *"Countries and Institutes in CTA Consortium"*. [Online; accessed 20-07-2018]. URL: https://www.cta-observatory.org/about/cta-consortium/.

[5] *"Shareholders and Associate Members of CTAO gGmbH"*. [Online; accessed 20-07-2018]. URL: https://www.cta-observatory.org/about/governance/.

[6] *CTA Requirements*. [Online; accessed 18-07-2018]. URL: https://jama.cta-observatory.org.

[7] Alison Mitchell and Jim Hinton. *SYS-REQ/180326: Photoelectrons to Photons in Camera Performance Requirements*. Internal Document (Draft V1.0). CTA Observatory, 2018.

[8] Stefan Ohm and Jim Hinton. *SCI-MC/121113: Impact of measurement errors on charge resolution and system performance*. Internal Document (V1.1). CTA Observatory, 2012.

[9] Karl Kosack et al. *CTA High-Level Data Model Definitions*. Internal Document (Draft V0.3). CTA Observatory, 2017.

[10] K. Bechtol et al. "TARGET: A multi-channel digitizer chip for very-high-energy gamma-ray telescopes". In: *Astroparticle Physics* 36.1 (2012), pp. 156–165. arXiv: 1105.1832. URL: http://dx.doi.org/10.1016/j.astropartphys.2012.05.016.

[11] F. Aharonian et al. "Calibration of cameras of the H.E.S.S. detector". In: *Astroparticle Physics* 22.2 (2004), pp. 109–125. arXiv: 0408145 [astro-ph].

[12] J. Holder and for the VERITAS Collaboration. "Exploiting VERITAS Timing Information". In: January (2005), pp. 383–386. arXiv: 0507450 [astro-ph]. URL: http://arxiv.org/abs/astro-ph/0507450.

[13] P Cogan and For The Veritas Collaboration. "Analysis of Flash ADC Data With VERITAS". In: *Methods* 0.1 (2007), p. 4. arXiv: 0709.4208. URL: http://arxiv.org/abs/0709.4208.

[14] Eric W. Weisstein. *"Cross-Correlation." From MathWorld–A Wolfram Web Resource*. [Online; accessed 20-07-2018]. URL: http://mathworld.wolfram.com/Cross-Correlation.html.

[15] *SciPy: Open source scientific tools for Python: scipy.ndimage.correlate1d.* [Online; accessed 20-07-2018]. URL: `https://docs.scipy.org/doc/scipy/reference/generated/scipy.ndimage.correlate1d.html`.

[16] J. Albert et al. "FADC signal reconstruction for the MAGIC telescope". In: *Nuclear Instruments and Methods in Physics Research, Section A: Accelerators, Spectrometers, Detectors and Associated Equipment* 594.3 (2008), pp. 407–419. arXiv: `0612385 [astro-ph]`.

[17] S. Klepser et al. "Hardware and software architecture of the upgraded H.E.S.S. cameras". In: *Proceedings of Science* (2017), pp. 0–8. arXiv: `1708.04550`.

[18] Raphaël Chalmé-Calvet et al. "Exploiting the time of arrival of Cherenkov photons at the 28 m H.E.S.S. telescope for background rejection: Methods and performance". In: *Proceedings of Science* 30-July-20 (2015). arXiv: `1509.03544`.